THE JOURNAL OF BIOLOGICAL CHEMISTRY VOL. 291, NO. 5, pp. 2469–2484, January 29, 2016

Regulation of the Water Channel Aquaporin-2 via 14-3-3θ and -ζ*

Received for publication, September 9, 2015, and in revised form, December 7, 2015 Published, JBC Papers in Press, December 8, 2015, DOI 10.1074/jbc.M115.691121

Hanne B. Moeller[‡], Joachim Slengerik-Hansen[‡], Takwa Aroankins[‡], Mette Assentoft[§], Nanna MacAulay[§], Soeren K. Moestrup[‡¶], Vivek Bhalla[‖], and Robert A. Fenton[‡1]

From the [‡]Department of Biomedicine and Center for Interactions of Proteins in Epithelial Transport, Aarhus University, 8000 Aarhus, Denmark, the [§]Department of Neuroscience and Pharmacology, Faculty of Health and Medical Sciences, University of Copenhagen, 2200 Copenhagen, Denmark, the [¶]Institute of Molecular Medicine, University of Southern Denmark, 5000 Odense, Denmark, and the [‖]Division of Nephrology, Department of Medicine, Stanford University, Palo Alto, California 94305

The 14-3-3 family of proteins are multifunctional proteins that interact with many of their cellular targets in a phosphorylation-dependent manner. Here, we determined that 14-3-3 proteins interact with phosphorylated forms of the water channel aquaporin-2 (AQP2) and modulate its function. With the exception of σ, all 14-3-3 isoforms were abundantly expressed in mouse kidney and mouse kidney collecting duct cells (mpkCCD$_{14}$). Long-term treatment of mpkCCD$_{14}$ cells with the type 2 vasopressin receptor agonist dDAVP increased mRNA and protein levels of AQP2 alongside 14-3-3β and -ζ, whereas levels of 14-3-3η and -θ were decreased. Co-immunoprecipitation (co-IP) studies in mpkCCD$_{14}$ cells uncovered an AQP2/14-3-3 interaction that was modulated by acute dDAVP treatment. Additional co-IP studies in HEK293 cells determined that AQP2 interacts selectively with 14-3-3ζ and -θ. Use of phosphatase inhibitors in mpkCCD$_{14}$ cells, co-IP with phosphorylation deficient forms of AQP2 expressed in HEK293 cells, or surface plasmon resonance studies determined that the AQP2/14-3-3 interaction was modulated by phosphorylation of AQP2 at various sites in its carboxyl terminus, with Ser-256 phosphorylation critical for the interactions. shRNA-mediated knockdown of 14-3-3ζ in mpkCCD$_{14}$ cells resulted in increased AQP2 ubiquitylation, decreased AQP2 protein half-life, and reduced AQP2 levels. In contrast, knockdown of 14-3-3θ resulted in increased AQP2 half-life and increased AQP2 levels. In conclusion, this study demonstrates phosphorylation-dependent interactions of AQP2 with 14-3-3θ and -ζ. These interactions play divergent roles in modulating AQP2 trafficking, phosphorylation, ubiquitylation, and degradation.

The 14-3-3 family are highly conserved proteins expressed in eukaryotic cells that play well established roles in interacting and modulating the function of target proteins at numerous levels (1–3). Seven 14-3-3 isoforms have been identified in mammalian cells (encoded by 7 different genes): β, ε, γ, η, σ, θ, and ζ. Each are functional as homo- or heterodimers, displaying high affinity binding via selective interaction motifs in their target proteins (1–3). Although 14-3-3 protein interactions are often dependent on the phosphorylation status of their target protein, with binding motifs commonly containing phosphorylated serine or threonine residues (1, 4, 5), binding motifs containing non-phosphorylated residues have also been identified (6). Once docked, 14-3-3 dimers have been proposed to regulate the function of their target proteins in various manners, including: 1) acting as an "adaptor" for modulating interaction between two target proteins that each bind to a 14-3-3 monomer; 2) mediating conformational changes to modulate target protein activity; and 3) competing with other interaction proteins to control post-translational modification and/or localization of the target protein (1, 7). Due to essential roles of 14-3-3 proteins in modulating signal transduction pathways and protein trafficking (2, 8), dysfunction of 14-3-3 proteins are linked to diseases including cancer (8, 9), metabolic disorders, and altered cell proliferation (10).

In the kidney, 14-3-3 proteins are expressed throughout the renal tubule (*e.g.* Refs. 11–13), including the principal cells of the kidney collecting duct (14). The primary functions of these cells are to regulate NaCl (via the epithelial sodium channel, ENaC)[2] and water (via the water channel aquaporin-2, AQP2) transport from the preurine back to the blood and help maintain body NaCl and water homeostasis. A role of 14-3-3 to modulate ENaC function and NaCl transport is well established (*e.g.* Refs. 15–18). The 14-3-3 isoforms β and ε constitutes a heterodimer that interacts with a phosphorylated form of the E3 ligase Nedd4-2, blocking the interaction of Nedd4-2 with ENaC, reducing ENaC ubiquitylation and thereby increasing apical ENaC density and sodium transport. Furthermore, the steroid hormone aldosterone, which increases ENaC function, also increases abundance of 14-3-3β and -ε; suggesting that 14-3-3 isoform abundance can be selectively modulated by various hormones. In respect to water transport, although 14-3-3θ and -ζ are associated with intracellular AQP2 vesicles in the inner medullary collecting duct (19), a role for 14-3-3 proteins in modulating AQP2 function is not established. AQP2 functions as a tetrameric protein with the carboxyl termini located

* This work was supported by the Danish Medical Research Council, the Lundbeck Foundation, the Novo Nordisk Foundation, the Carlsberg Foundation, MEMBRANES, and the Aarhus University Research Foundation. The authors declare that they have no conflicts of interest with the contents of this article.

[1] To whom correspondence should be addressed: Bldg. 1233, Rm. 213, Wilhelm Meyers Allé 3, 8000 Aarhus C, Denmark. Tel: 004587167671; E-mail: robert.a.fenton@biomed.au.dk.

[2] The abbreviations used are: ENaC, epithelial sodium channel; AQP2, aquaporin-2; OA, okadaic acid; CA, calyculin A; dDAVP, [deamino-Cys[1],D-Arg[8]]vasopressin; IP, immunoprecipitation; SPR, surface plasmon resonance; IMCD, inner medulla collecting duct; AVP, arginine vasopressin; qRT, quantitative RT.

inside the cell (20). This tail domain is highly phosphorylated, with the levels of phosphorylation at Ser-256, Ser-261, Ser-264, and Ser-269 (Thr in human) residues being modulated by the hormone arginine vasopressin (AVP) (21, 22), acting via the vasopressin type 2 receptor (V2R). These phosphorylation sites play alternative roles in the subcellular distribution and function of AQP2, *e.g.* the apical plasma membrane accumulation of AQP2 in response to AVP treatment is modulated by Ser-256 and Ser-269 phosphorylation (23–28). Although the underlying mechanisms for AQP2 regulation via phosphorylation are not completely clear, phosphorylation-dependent protein interactions appear to play a crucial role (29). In addition, the carboxyl-terminal tail of AQP2 is further modified by ubiquitylation (30). A complex interplay between AQP2 phosphorylation and ubiquitylation is responsible for modulating the abundance of AQP2 on the plasma membrane (23).

In this study, we tested the hypothesis that AQP2 function is regulated by interaction with 14-3-3 proteins and that these interactions are modulated by AVP. In mouse kidney and a collecting duct cell line (mpkCCD$_{14}$), 14-3-3 isoforms were identified at the mRNA and protein levels, several of which were modified in abundance by AVP. These 14-3-3 isoforms had alternative subcellular distributions in mouse kidney collecting duct cells. Biochemical studies identified an AVP-regulated and phosphorylation-dependent interaction between AQP2 and 14-3-3θ and -ζ. Knockdown of θ and ζ in mpkCCD$_{14}$ cells indicated that θ reduces AQP2 trafficking to the plasma membrane, whereas ζ prevents AQP2 ubiquitylation and degradation. Our data provide additional evidence that AQP2 function is highly dependent on phosphorylation-dependent protein interactions with its carboxyl-terminal domain.

Experimental Procedures

Antibodies and Chemicals—Affinity-purified rabbit phospho-specific antibodies against Ser(P)-269-AQP2 or against total AQP2 upstream of known phosphorylation sites have previously been characterized (21, 24). Rabbit anti-V2R has been characterized previously (31). Mouse anti-ubiquitin (P4D1) was from Cell Signaling. Total 14-3-3 antibodies (catalog numbers sc629 and sc1657) were from Santa Cruz. 14-3-3 isoform-specific antibodies β (number 9636), ϵ (number 9635), γ (number D15B7), η (number D23B7), θ (number 9638), and ζ (number 7413) were from Cell Signaling. Anti-HA tag (H3663), GST (number G1160), and α-tubulin (T6074) were from Sigma. The phosphatase inhibitors okadaic acid (OA) and calyculin A (CA) were from Calbiochem. Forskolin (Sigma) was used at a final concentration of 25 μM.

Tissue Isolation from Mice—All animal protocols comply with the European Community guidelines for the use of experimental animals and were performed in accordance to licenses for the use of experimental animals issued by the Danish Ministry of Justice. Mice were euthanized by cervical dislocation, kidneys were removed and dissected into cortex and inner medulla regions. Tissue was either processed for RNA extraction (see below) or homogenized in ice-cold isolation solution (250 mM sucrose, 10 mM triethanolamine, pH 7.6, containing the protease inhibitors leupeptin (1 mg/ml) and Pefa-block (0.1 mg/ml) (Roche Applied Science) and phosphatase inhibitor mixture tablets (PhosSTOP, Roche Diagnostics A/S)) for generation of SDS-PAGE gel samples.

Immunohistochemical Labeling of Mouse Kidney and Confocal Imaging—Kidneys were perfused with 4% paraformaldehyde in PBS via the heart and post-fixed for 60 min in the same buffer. Tissue was immersed in 20% sucrose in PBS at 4 °C overnight and rapidly frozen using liquid nitrogen. 10-μm sections were cut, placed on Superfrost Plus slides, and heated to 60 °C for 10 min. After 30 min incubation in 50 mM NH_4Cl in PBS to quench aldehydes, sections were dehydrated and rehydrated through a series of alcohol (70, 96, 99, 96, and 70%). The fluorescent labeling procedure was performed as previously described (24). Coverslips were mounted with a hydrophilic mounting medium containing anti-fading reagent (DAKO, glycergel). A Leica TCS SL confocal microscope with an HCX PL APO ×63 oil objective lens (numerical aperture: 1.40) was used for obtaining images.

mpkCCD$_{14}$ Cell Culture and Experimental Conditions—mpkCCD$_{14}$ cells were cultured as described (32) on semi-permeable supports (0.4 μM pore size, Corning) until a confluent monolayer formed and TER was above 5 kOhm/cm^2. Where indicated, the AVP type II receptor selective agonist [deamino-Cys^1,D-Arg^8]vasopressin (dDAVP) (10^{-9} M, Sigma) was added in serum-free media to the basolateral compartment for 24–96 h to induce AQP2 expression. For experiments requiring acute dDAVP stimulation, cells were washed twice in pure media and reincubated in pure media for 3 h before re-stimulated with dDAVP (10^{-9} M) from the basolateral side for 20 min at 37 °C. In dDAVP washout experiments, cells were subsequently washed twice in pure media and reincubated for 30 min at 37 °C before sample preparation. In phosphatase inhibitor experiments, where indicated OA (200 nM) and CA (100 nM) were included during the washout period. For cycloheximide chase studies, cells were grown in dDAVP for 4 days on semi-permeable supports, following which cells were incubated for various time points at 37 °C and 5% CO_2 in 50 μM cycloheximide (in dimethyl sulfoxide). Cells were washed twice in PBS and proteins were extracted in Laemmli sample buffer containing 10 mg/ml of DTT. For calculation of the protein half-life, average band densities for each time point were normalized to control and fitted using nonlinear regression and a one-phase exponential decay equation using GraphPad Prism software. Data were obtained from four independent experiments, with 3–6 observations for each individual time point.

Transduction of 14-3-3 Lentivirus—MISSION lentiviral transduction particles against 14-3-3θ (numbers 76393, 76394, 312369, 312371, and 349888) and -ζ (numbers 71053, 71054, 71056, 71057, and 316456) and corresponding control particles (SHC002) were from Sigma. mpkCCD$_{14}$ cells were cultured as described (32) in 6-well plates until 95% confluent. Cells were treated with hexadimethrine bromide (8 μg/ml final concentration) for 15 min in pure media, before addition of lentiviral particles (multiplicity of infection = 4). Transduction was allowed to proceed for 24 h, after which media was switched to mpkCCD$_{14}$ media containing 2 μg/ml of puromycin for selection. Multiple clonal cell lines were isolated and individually characterized by examination of cell morphology, high TER

when grown on semi-permeable supports, and 14-3-3 expression levels by Western blotting and qRT-PCR.

Surface Biotinylation of mpkCCD$_{14}$ Cells—Apical plasma membrane proteins were labeled with EZ-link hydrazide-biocytin (Pierce), which reacts with oxidized glycans of glycosylated proteins, using a modified published protocol (33, 34). Following various experimental manipulations, cells were washed in ice-cold coupling buffer (sodium phosphate, 0.1 M; NaCl, 0.15 M, pH 7.2) and incubated with sodium metaperiodate (20 mM) in coupling buffer for 30 min on ice in the dark. After washes in coupling buffer, cells were incubated from the apical side using 2.5 mM hydrazide-biocytin for 30 min on ice. Subsequently, cells were incubated with quenching solution (NH_4Cl, 50 mM, in PBS, pH 7.4) for 5 min and washed in coupling buffer. Cells were lysed in a buffer containing: 50 mM Tris, pH 7.5, 140 mM NaCl, 5 mM $CaCl_2$, 5 mM $MgCl_2$, 1% Nonidet P-40 supplemented with EDTA-free Halt Protease and Phosphatase Inhibitor Mixture (Invitrogen). Samples were purified as described previously (29), with labeled proteins eluted by incubation in Laemmli sample buffer containing 10 mg/ml of DTT for 10 min at 95 °C.

Immunoprecipitation (IP) Using mpkCCD$_{14}$ Cells—Immunoprecipitation was performed as previously described (23).

HEK Cell Culture, Transfection, and Immunoprecipitation—HEK293 cells (ATCC CRL-1573) were cultured at 37 °C and 5% CO_2 in Dulbecco's modified Eagle's medium/GlutaMAX (Invitrogen) supplemented with 10% donor bovine serum, 100 IU/ml each of penicillin and streptomycin in 6-well plates until 95% confluent. Cells were transfected with AQP2 (21) and various HA-tagged 14-3-3 constructs (16) using Lipofectamine 2000 reagent (Invitrogen) following standard procedures. After 36 h, cells were washed in ice-cold PBS-CM, pH 8.0 (PBS containing 1 mM $CaCl_2$ and 0.1 mM $MgCl_2$), and incubated with forskolin (1 μM final) for 15 min before addition of lysis buffer (50 mM Tris, pH 7.5, 140 mM NaCl, 5 mM $CaCl_2$, 5 mM $MgCl_2$, 1% Nonidet P-40) containing EDTA-free Halt Protease and Phosphatase Inhibitor Mixture (Invitrogen). Immunoprecipitations were performed for 2 h at room temperature on equal protein quantities of cleared lysates using Protein A/G Dynabeads (Invitrogen). Extensive washes were performed using lysis buffer and captured proteins were eluted using Laemmli sample buffer containing 10 mg/ml of DTT. All immunoprecipitation assays were repeated twice with different batches of transfected cells, but yielded similar results.

Specificity of 14-3-3 Isoform Selective Antibodies—HEK293 cells were transfected with various HA-tagged 14-3-3 constructs (16) using Lipofectamine 2000 reagent (Invitrogen) following standard procedures. After 36 h cells were washed twice in PBS and proteins were extracted in Laemmli sample buffer containing 10 mg/ml of DTT before blotting with various isoform-selective antibodies.

GST Pulldown Assay—mpkCCD$_{14}$ cells were treated with dDAVP for 30 min and lysates were prepared as described under "HEK Cell Immunoprecipitations," as described above. Lysates were pre-cleared by incubation with 100 μl of glutathione-agarose (Thermo Scientific) for 120 min at 4 °C. GST-14-3-3 fusion constructs (Sino Biological Inc.) were purified using Zeba spin columns (Thermo Scientific) to remove excess glutathione. 30 μg of each construct was immobilized on glutathione-agarose (Thermo Scientific) following the manufacturer's guidelines. 14-3-3-Labeled beads or control beads were incubated in TBS containing EDTA-free Halt Protease and Phosphatase Inhibitor Mixture (Invitrogen) overnight at 4 °C. After extensive washing in TBS, captured proteins were eluted by 2 × 15 min incubation with 10 mM glutathione, followed by a single elution using Laemmli sample buffer. All GST pulldown assays were repeated twice with different lysates, but yielded similar results.

Surface Plasmon Resonance (SPR) Analyses—A potential direct interaction between 14-3-3 and various AQP2 peptides corresponding to the last 44 amino acids of mouse AQP2 in either unmodified, or phosphorylated at single sites corresponding to Ser-256, Ser-264, or Ser-269 (Genscript, USA) was studied by SPR analysis on a Biacore 3000 instrument, essentially as described (35). Biacore type CM5 sensor chips were activated with a 1:1 mixture of 0.2 M *N*-ethyl-*N*′-(3-dimethylaminopropyl)carbodiimide and 0.05 M *N*-hydroxysuccimide in water according to instructions by the manufacturer. GST-14-3-3θ (Sino Biological Inc.) was immobilized in 10 mM sodium acetate, pH 4.0, and the remaining binding sites were blocked with 1 M ethanolamine, pH 8.5. A control flow cell was made by performing the activation and blocking procedure only. Peptides were dissolved in 10 mM Hepes, 150 mM NaCl, 2.0 mM $CaCl_2$, 1.0 mM EGTA, and 0.005% Tween 20, pH 7.4. Sample and running buffers were identical. Regeneration of the sensor chip after each analysis cycle was performed with 10 mM glycine, pH 4.0, containing 20 mM EDTA and 500 mM NaCl.

14-3-3 Far Western Blotting (Overlay Assay)—mpkCCD$_{14}$ cells were grown in dDAVP for 4 days, treated acutely with dDAVP where indicated (description above), and AQP2 was immunoprecipitated as previously described (23). Some samples were solubilized with 1% SDS for 10 min with heating at 60 °C, after which the SDS was diluted to 0.1% using lysis buffer before IP. IP samples, alongside various AQP2 peptides were separated by SDS-PAGE and transferred to PVDF membrane. Membranes were blocked in 5% skimmed milk in TBST for 1 h at room temperature, before incubation overnight at 4 °C with 1 μg/ml of GST 14-3-3ζ (Sino Biological Inc.) in 5% BSA in TBST. After washing in TBST, membranes were incubated at room temperature for 1 h with an HRP-linked GST antibody (number A00866, Genscript) before visualization using ECL detection.

RT-PCR and Real Time qRT-PCR—Total RNA was isolated using the Ambion Ribopure kit (Invitrogen), treated with DNase I (Invitrogen), and reverse transcribed using Superscript II and random primers (Invitrogen); all steps were performed according to the manufacturer's instructions. A control reaction without the reverse transcriptase enzyme was performed to exclude genomic DNA amplification. Primer pairs utilized were: AQP2 (5′-TGGCTGTCAATGCTCTCCAC and 5′-GGAGCAGCCGGTGAAATAGA); 18S RNA (5′-GGATCCATTGGAGGGCAAGT and 5′-ACGAGCTTTTTAACTGCAGCAA); 14-3-3β (5′-TGGATAAGAGTGAGCTGGTACA and 5′-CGTGTCCCTGCTCTGTTACG); 14-4-4ϵ (5′-AGTGACATTGCGATGACAGAAC and 5′-ACGGTCGGGGGAATTAAGAAT); 14-3-3γ (5′-CCAAGAGGCGTTTGATATAAGCA and AAAAGCCGTTTTAGCCAGTGT), 14-3-3η (5′-

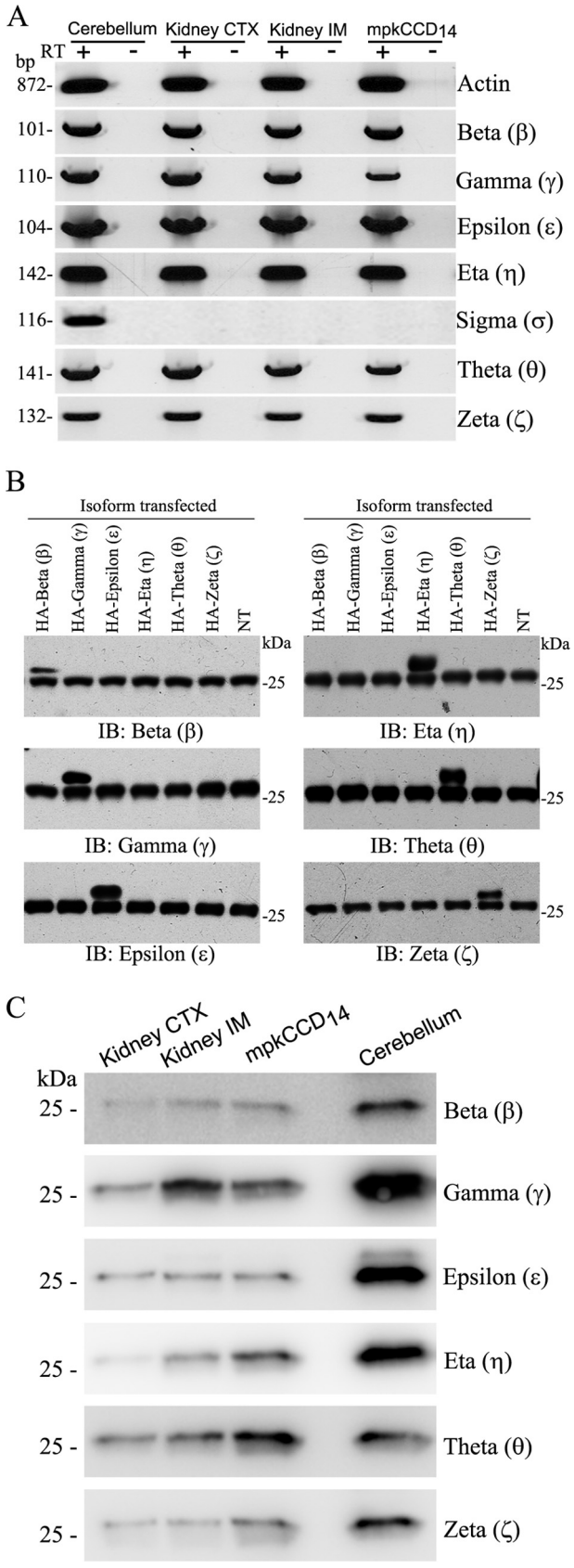

FIGURE 1. **Identification of 14-3-3 isoforms in mpkCCD$_{14}$ cells and mouse kidney.** *A,* RT-PCR using mouse 14-3-3 isoform-specific primers on mouse cerebellum, mpkCCD$_{14}$ cells, mouse kidney cortex (*CTX*), and inner medulla (*IM*). Primers against actin were used as a positive control. All 14-3-3 isoforms with the exception of σ were detected. *B,* specificity of 14-3-3 isoform-selective antibodies. HEK cells were transfected with various HA-tagged 14-3-3 isoforms followed by Western blotting on cell lysates using 14-3-3 isoform-selective antibodies. In HEK cells, the endogenous levels of all isoforms are relatively high. Using the various isoform selective antibodies, an additional higher molecular weight band representing the HA tag form of 14-3-3 was identified only using corresponding antibodies. *C,* immunoblotting of mouse cerebellum, mpkCCD$_{14}$ cells, mouse kidney cortex (*CTX*), and inner medulla (*IM*) protein homogenates using 14-3-3 isoform-specific antibodies confirmed the RT-PCR results.

ACGAAGATCGAAATCTCCTCTCT and 5′-CCGGTAGGCTTTAACTTTCTCCA); 14-3-3σ (5′-TGTGTGCGACACTGTGCTC and 5′-TCGGCTAGGTAGCGGTAGTAG), and 14-3-3ζ (5′-AAAAGTTCTTGATCCCCAATGC and 5′-TGTGACTGGTCCACAATTCCTT) spanned an exon-exon junction or an intron. β-Actin was used as a positive control for cDNA integrity and cDNA from mouse cerebellum was used as a positive control for 14-3-3 isoform amplification. Specificity of the amplified products was determined using melting curve-analysis software, gel electrophoresis, and sequencing. Amplification was performed using the cDNA equivalent of 5 ng of RNA, 5 pmol of each primer and either HotStar *Taq* polymerase (Qiagen) or SYBR Green I Master *Taq* (Roche Applied Science). Cycling conditions were: 95 °C for 5 min, followed by 40 cycles of 95 °C for 10 s, 62 °C for 20 s, and 72 °C for 30s. qRT-PCR reactions were run on a LightCycler 480 (Roche), with fluorescence measured at the end of each elongation step to calculate C_t values. Relative quantitation of gene expression was determined using the comparative C_t method, with validation experiments performed to determine that amplification efficiencies were equal between control and experimental groups. Signals for ribosomal 18S amplified in parallel were used to normalize for differences in the amount of starting cDNA.

Immunoblotting—Standard procedures were utilized for sample preparation and SDS-PAGE. Immunoblots were developed using ECL detection and signal intensity in specific bands were quantified using Image Studio Lite (Qiagen) densitometry analysis.

Statistics—All quantitative experiments on cultured cells were performed on at least 2 wells of cells in 3 different experiments. Data were tested for normal distribution using the D'Agostino-Pearson omnibus test and GraphPad Prism Software. Data fitting a normal distribution were analyzed using one-way analysis of variance followed by Tukey's Multiple Comparison Test. Multiple comparison tests were applied only when a significant difference ($p < 0.05$) was determined in the analysis of variance. Data not fitting a normal distribution were assessed using a nonparametric Kruskal-Wallis test. All data are presented as mean ± S.E.

Results

14-3-3 Isoforms in mpkCCD$_{14}$ Cells and Mouse Kidney—Initial RT-PCR using mouse isoform-specific primers determined that all known 14-3-3 isoforms, with the exception of σ, were present at high levels in mpkCCD$_{14}$ cells and mouse kidney cortex and inner medulla (Fig. 1*A*). To confirm the expression of 14-3-3 isoforms (except σ) at the protein level, isoform-specific antibodies were utilized. HEK cells transfected with various HA-tagged 14-3-3 isoforms followed by Western blotting on cell lysates confirmed that the endogenous levels of all iso-

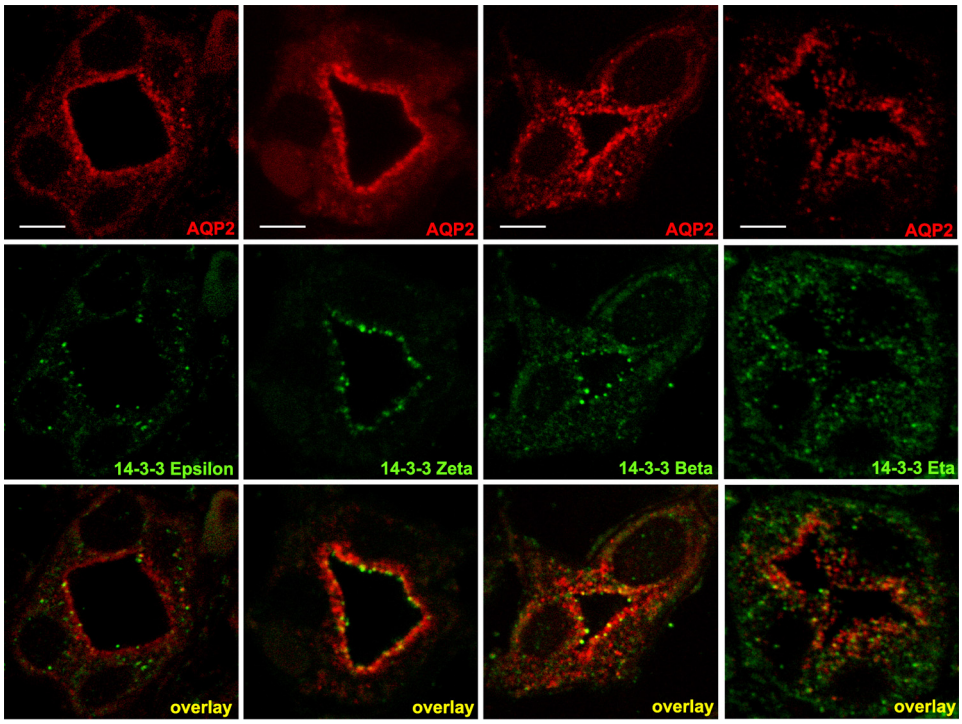

FIGURE 2. **Subcellular distribution of AQP2, 14-3-3ϵ, -ζ, -β, and -η in mouse kidney IMCD cells.** Isoform-specific antibodies were utilized on cryosections of mouse kidney. The various 14-3-3 isoforms (*green*) had alternative punctuate distributions in IMCD cells. 14-3-3ζ had a similar distribution similar to AQP2 at the apical plasma membrane. *Scale bar* is 10 μm.

forms in HEK cells are relatively high, and that the antibodies utilized were isoform specific (Fig. 1*B*). In mouse kidney cortex, inner medulla, and mpkCCD$_{14}$ cell homogenates, endogenous expression of all 14-3-3 isoforms identified at the message level were confirmed (Fig. 1*C*).

Similar isoform-specific antibodies were used to examine the subcellular distribution of various 14-3-3 proteins in mouse kidney inner medulla collecting duct (IMCD) cells. Technical issues prevented analysis of the antibodies using formaldehyde-fixed paraffin-embedded tissue (not shown). After optimization, some of the antibodies worked successfully using cryosections (Fig. 2). Each of the isoforms detected successfully using immunohistochemistry had various and punctuate distributions in IMCD cells, suggesting distinct roles. Although 14-3-3β, -ϵ, and -η were predominantly distributed throughout the cytoplasm, 14-3-3ζ was localized near the apical plasma membrane, with a distribution similar to AQP2.

Regulation of 14-3-3 Isoform Abundance by AVP—mpkCCD$_{14}$ cells were grow on semi-permeable supports and treated for 24, 48, or 72 h with dDAVP. qRT-PCR was performed using mouse 14-3-3 isoform-selective primers. dDAVP treatment significantly increased AQP2 mRNA levels relative to controls from 24 to 72 h (Table 1). Concerning the isoforms, mRNA increased for the β (24–72 h) and ζ (48–72 h) isoforms, whereas mRNA for η (24–74 h) and θ (48–72 h) isoforms were decreased. AQP2 and 14-3-3 protein levels were examined using the isoform-specific antibodies and a similar experimental set-up (Fig. 3). AQP2 protein levels increased from 24 to 72 h. In alignment with the mRNA data, protein levels of 14-3-3β (24–72 h) and -ζ (48–72 h) isoforms were significantly increased by dDAVP, whereas η (24–74 h) and θ (72 h) protein abundances were significantly decreased following dDAVP treatment.

AQP2 Co-immunoprecipitates with 14-3-3 in mpkCCD$_{14}$ Cells—To test the hypothesis that 14-3-3 and AQP2 interact, IP studies on mpkCCD$_{14}$ cell lysates were performed. After optimization of experimental conditions (alterations in divalent cation concentration and detergent type/concentration in lysis buffer, data not shown), a reproducible AQP2 and 14-3-3 interaction was identified (Fig. 4). AQP2 could be detected in samples immunoprecipitated using either an AQP2-specific antibody (Fig. 4*A*), or with an antibody targeting total 14-3-3 (does not differentiate between isoforms), but not with an AQP1-specific antibody (negative control). Similarly, 14-3-3 could be detected in 14-3-3 or AQP2 IP samples, but not AQP1 IP samples (Fig. 4*B*).

AQP2 Interaction with 14-3-3 Is Regulated by AVP—To examine if the AQP2 and 14-3-3 interaction was regulated by AVP, mpkCCD$_{14}$ cells were cultured in dDAVP for 3 days (to increase AQP2 levels), followed by acute stimulation with dDAVP (see "Experimental Procedures"). Following 20 min dDAVP stimulation, the interaction between AQP2 and 14-3-3 was enhanced, with a greater quantity of 14-3-3 immunoisolated using an AQP2 antibody, or conversely, a greater quantity of AQP2 immunoisolated using a 14-3-3 antibody (Fig. 5*A*). Quantification data from 3 individual immunoprecipitations is shown in Fig. 5, *B* and *C*.

AVP Washout in the Presence of Phosphatase Inhibitors Preserves the AQP2 and 14-3-3 Interaction—We previously determined that several AQP2 protein/protein interactions are dependent on the phosphorylation status of AQP2 at Ser-256 and Ser-269 (29) and that the phosphorylation of AQP2 (particularly at Ser-269) can be enhanced and prolonged during AVP washout by inhibition of specific protein phosphatases using OA and CA (23). To examine a potential role of phosphoryla-

TABLE 1

Effects of long term dDAVP (1 ng) treatment of mpkCCD cells on AQP2 and 14-3-3 isoform mRNA levels

Data are mean ± S.E. from semi-qRT-PCR studies.

	24 h		48 h		72 h	
	Control	dDAVP	Control	dDAVP	Control	dDAVP
AQP2	1.00 ± 0.00	1.72 ± 0.16[a]	1.01 ± 0.17	3.03 ± 0.19[a,b]	1.17 ± 0.16	3.10 ± 0.34[a]
14-3-3β	1.00 ± 0.00	1.54 ± 0.20[a]	1.03 ± 0.18	1.62 ± 0.17[a]	0.83 ± 0.13	1.75 ± 0.22[a]
14-3-3γ	1.00 ± 0.00	1.04 ± 0.19	0.95 ± 0.19	1.01 ± 0.21	0.96 ± 0.23	0.96 ± 0.17
14-3-3ϵ	1.00 ± 0.00	1.01 ± 0.11	0.99 ± 0.07	0.97 ± 0.07	0.96 ± 0.11	1.02 ± 0.08
14-3-3η	1.00 ± 0.00	0.70 ± 0.09[a]	0.99 ± 0.10	0.55 ± 0.08[a]	1.07 ± 0.11	0.58 ± 0.16[a]
14-3-3θ	1.00 ± 0.00	1.05 ± 0.10	0.99 ± 0.05	1.35 ± 0.04[a]	1.01 ± 0.08	1.69 ± 0.04[a,b]
14-3-3ζ	1.00 ± 0.00	1.00 ± 0.09	0.94 ± 0.12	0.75 ± 0.07[a]	0.97 ± 0.07	0.57 ± 0.09[a]

[a] Indicates $p < 0.05$ compared to the time-matched control group.
[b] Indicates $p < 0.05$ compared to the previous time point of treatment.

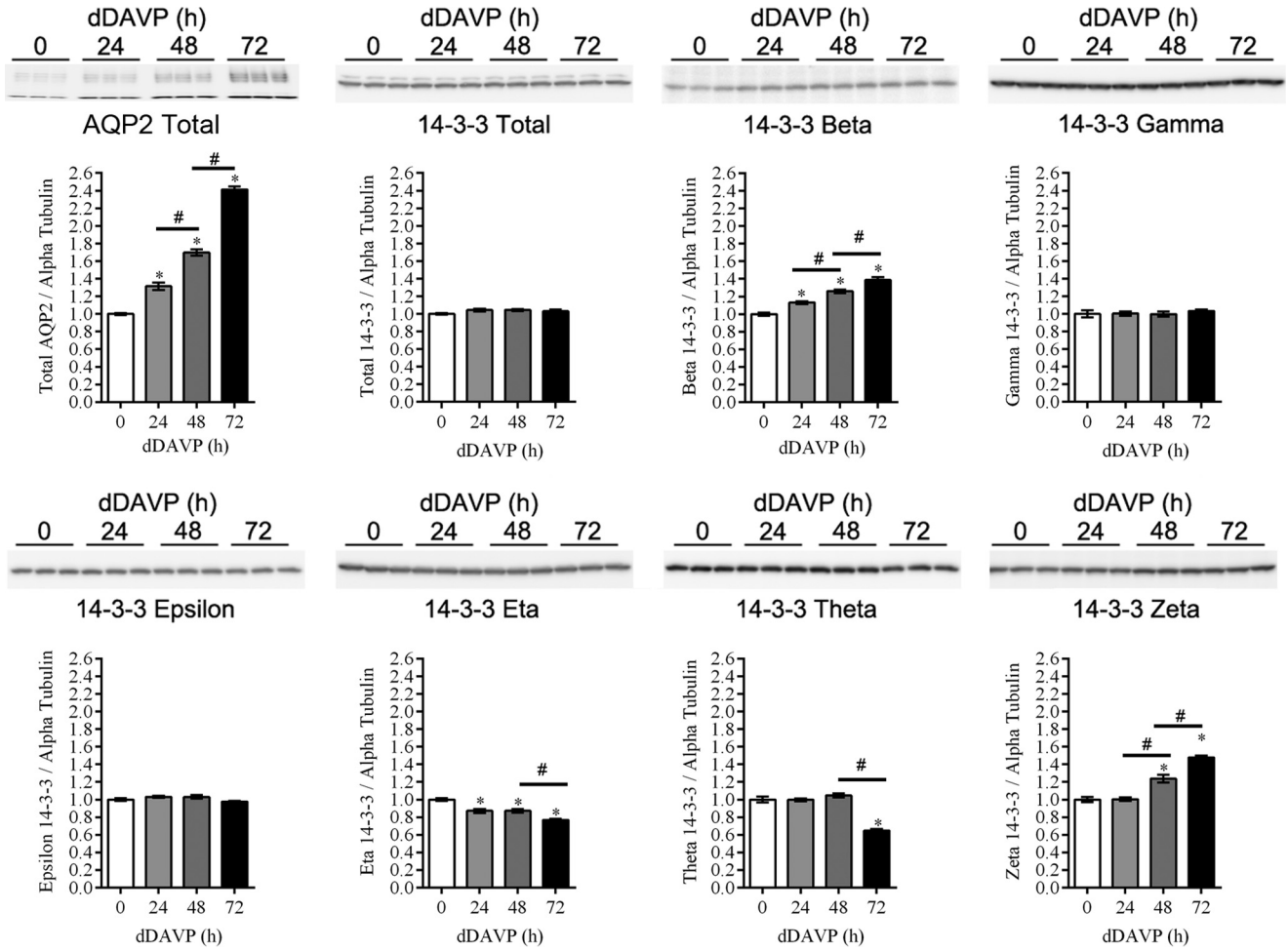

FIGURE 3. **Regulation of AQP2 and 14-3-3 isoform abundance by AVP.** mpkCCD$_{14}$ cells were grown on semi-permeable supports and treated for 24, 48, or 72 h with dDAVP followed by immunoblotting with AQP2 or various 14-3-3 isoform selective antibodies. * indicates $p < 0.05$ relative to the control condition. # indicates $p < 0.05$ from the group as indicated.

tion in mediating the interaction between AQP2 and 14-3-3, mpkCCD$_{14}$ cells were acutely stimulated with dDAVP followed by a washout period in the presence or absence of OA and CA. Similarly to what has been observed in MDCK cells (23), AQP2 Ser(P)-269 levels in mpkCCD$_{14}$ total cell lysates were significantly higher after acute dDAVP treatment, but were subsequently reduced following dDAVP washout (Fig. 6, *A* and *B*). However, AQP2 Ser(P)-269 levels remained significantly higher after dDAVP washout in the presence of CA and OA. Immunoprecipitations on the same cell lysates demonstrated once again a 14-3-3/AQP2 interaction that was enhanced following dDAVP stimulation (compare Figs. 5 and 6*A*). Although this interaction was reduced following dDAVP washout, the interaction remained significantly higher if the washout was performed in the presence of CA and OA (Fig. 6*C*).

14-3-3θ and -ζ Interact with AQP2—Technical issues (same species antibodies) prevented us performing a co-IP using the isoform-selective antibodies. Therefore, to determine which isoforms of 14-3-3 may interact with AQP2, HEK293T cells (do not express AQP2) co-transfected with various HA-14-3-3 constructs and AQP2 were stimulated with forskolin (to mimic dDAVP-induced increases in cAMP) followed by immunopre-

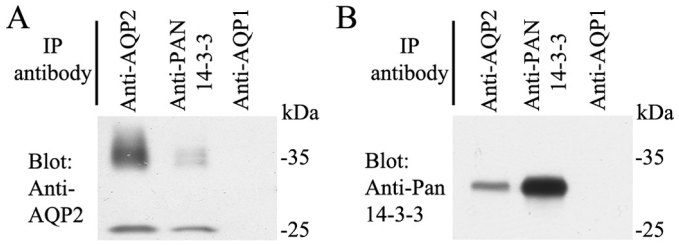

FIGURE 4. **AQP2 interaction with 14-3-3 in mpkCCD$_{14}$ cells.** *A,* a representative immunoblot from samples immunoprecipitated from mpkCCD$_{14}$ cell lysates using an AQP2-specific antibody. Both total 14-3-3 and AQP2 could be detected. *B,* a representative immunoblot from samples immunoprecipitated using a 14-3-3 specific antibody. Both total AQP2 and 14-3-3 could be detected. Neither 14-3-3 or AQP2 were detected in samples immunoprecipitated with AQP1 (negative control).

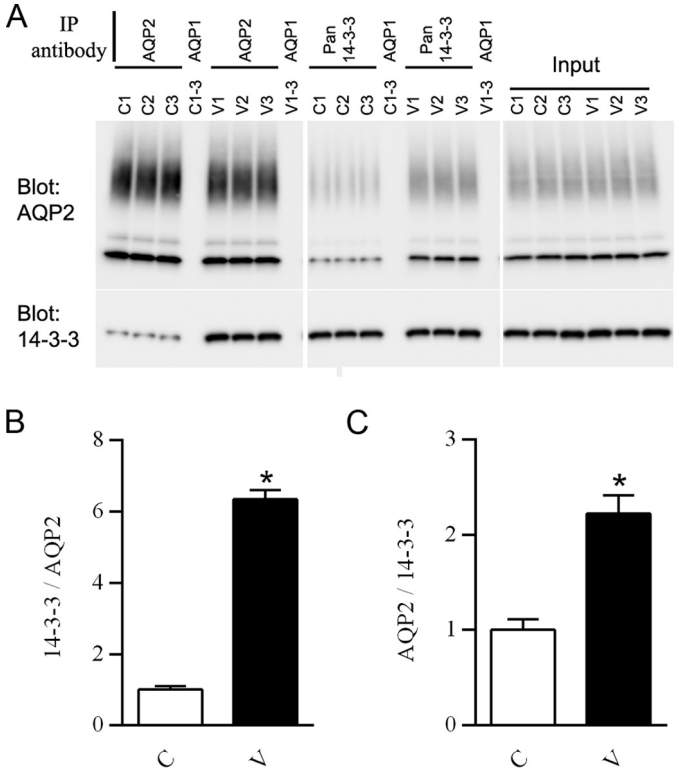

FIGURE 5. **AQP2 interaction with 14-3-3 is regulated by AVP.** Immunoprecipitations were performed on lysates from mpkCCD$_{14}$ cells cultured in dDAVP for 3 days, followed by acute stimulation with dDAVP for 20 min. *A,* representative immunoblotting of control conditions (*C*) or following acute dDAVP stimulation (*V*). Each *lane* represents a separate immunoprecipitation using antibodies as highlighted. *B* and *C,* summary quantification data of immunoprecipitations demonstrates the enhanced interaction between AQP2 and 14-3-3 following dDAVP treatment. * indicates $p < 0.05$ relative to the control condition.

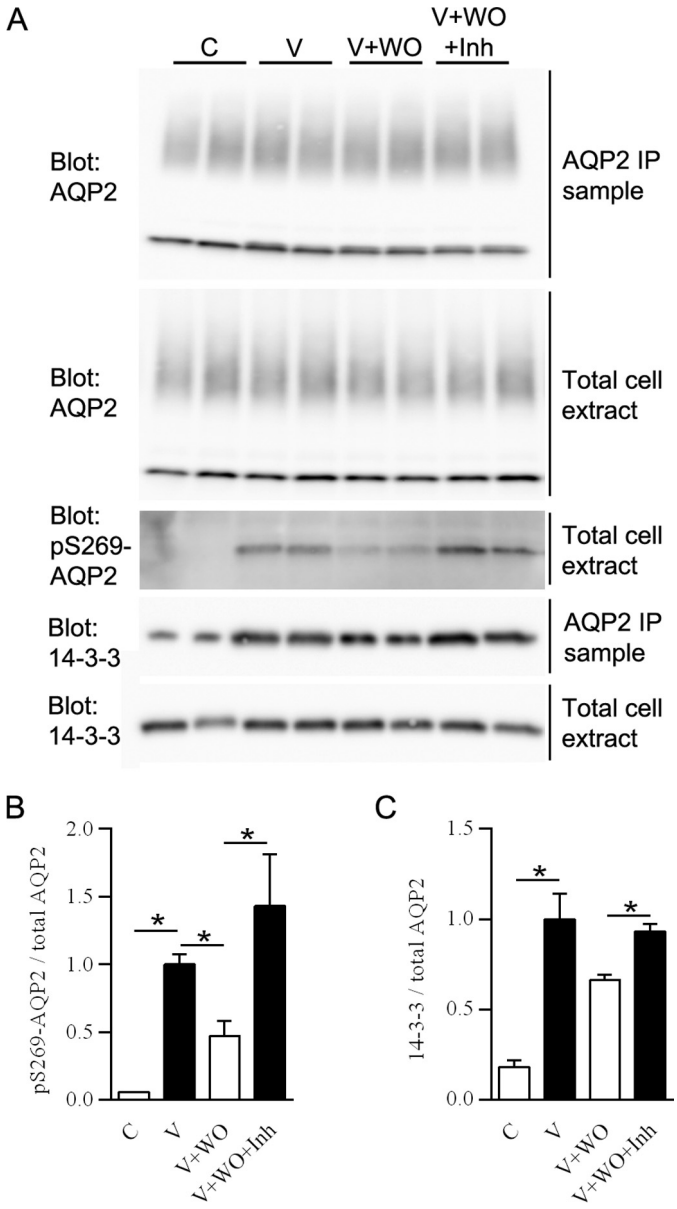

FIGURE 6. **AVP washout in the presence of phosphatase inhibitors preserves the AQP2 and 14-3-3 interaction.** mpkCCD$_{14}$ cells were acutely stimulated with dDAVP followed by a washout period in the presence or absence of the inhibitors okadaic acid and calyculin A. Immunoprecipitation was performed using AQP2. *A,* representative immunoblotting demonstrated a 14-3-3 and AQP2 interaction that was enhanced following dDAVP stimulation (*V*) relative to control (*C*). This interaction was reduced following dDAVP washout (*WO*), but remained significantly higher in the presence of inhibitors (*Inh*). AQP2 Ser(P)-269 levels in cell lysates followed a similar trend. *B* and *C,* summary quantification data of Ser(P)-269 AQP2 levels and 14-3-3/AQP2 interaction under the different experimental conditions. * indicates $p < 0.05$ relative to the control condition or from the group as indicated.

cipitation (Fig. 7). Similar to mpkCCD$_{14}$ cells, in AQP2 expressing HEK293 cells, AQP2 was detected in immunoprecipitates using a pan 14-3-3 antibody (detects all 14-3-3 isoforms). However, only in HEK293T cells expressing HA-14-3-3θ or -ζ was it possible to co-IP AQP2 using an anti-HA antibody, suggesting that AQP2 interacts selectively with these 14-3-3 isoforms (Fig. 7, *lower panel*). To confirm these potential selective interactions, we performed GST pulldown assays with 14-3-3ϵ, -θ, and -ζ as bait and dDAVP-treated mpkCCD$_{14}$ cell lysates as prey (Fig. 8). Non-coated control beads or 14-3-3ϵ-coated beads displayed no interactions with AQP2 (Fig. 8*A*). In contrast, AQP2 was consistently identified in eluates from either 14-3-3θ- or -ζ-coated beads (Fig. 8, *B* and *C*), suggesting that AQP2 selectively interacts with these isoforms directly. AQP2 was not identified in eluates from similar GST pulldown assays when the mpkCCD$_{14}$ cell lysate prey was preincubated with λ-protein phosphatase 1 for 60 min (not shown), indicating a role of phosphorylation in the AQP2/14-3-3 interaction.

Phosphorylation of AQP2 at Ser-256 Is Critical for 14-3-3 Interactions—AQP2 contains four highly conserved and AVP-regulated phosphorylation sites at Ser-256, Ser-261, Ser-264,

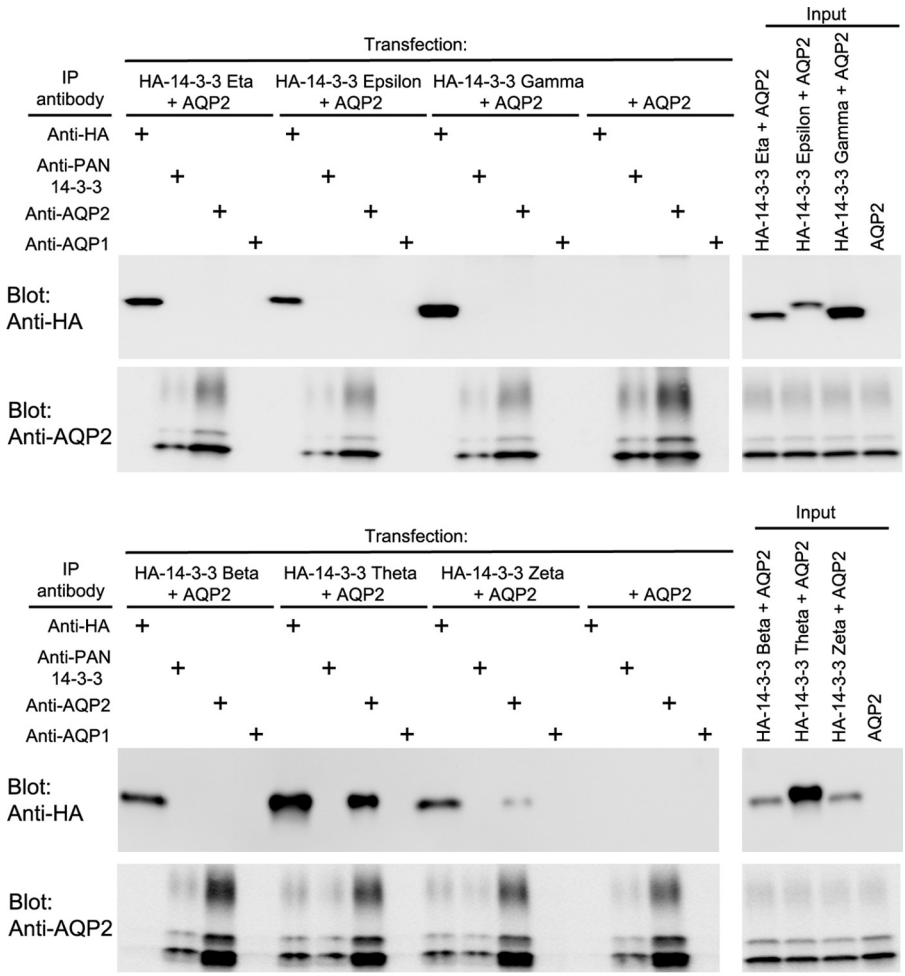

FIGURE 7. **14-3-3θ and -ζ interact with AQP2 in HEK293T cells.** HEK293T cells were co-transfected with various HA-14-3-3 constructs and AQP2, stimulated with forskolin and subject to immunoprecipitation with various antibodies. In immunoprecipitates using a total 14-3-3 antibody, AQP2 was detected. However, only in HEK293T cells expressing HA-14-3-3θ or -ζ immunoprecipitated using an anti-HA antibody was AQP2 identified, suggesting that AQP2 interacts selectively with these 14-3-3 isoforms.

and Ser-269 (Thr in human) at its carboxyl-terminal tail. Although early analysis of 14-3-3 interactions proposed three fundamental binding motifs (or criteria) within target phosphoproteins: 1) RSX(pS)XP (mode I); 2) RX(F/Y)*X*(pS)XP (mode II) and; 3) a phosphorylated residue as the penultimate residue in the carboxyl-terminal tail of the protein target (5, 36), subtle variations of these motifs make prediction of 14-3-3 binding sites difficult. Recently, based on the observations that the majority of human 14-3-3 interacting phosphoproteins are 2R-ohnologues (37), new methods have been developed to predict 14-3-3-binding phosphosites using a variety of algorithms (38). Analysis of human AQP2 scored highly the region surrounding the Ser-256 site of AQP2 (EVRRRQpSVELH) as a 14-3-3 interacting motif using three complimentary methods (scores: artificial neural network = 0.742 (cut-off = 0.55); position-specific scoring matrix = 1.155 (cut-off = 0.80); support vector machine = 0.616 (cut-off = 0.25); consensus = 0.838 (cut-off = 0.50)). Similar high scores were obtained using mouse or rat AQP2 for analysis. These bioinformatics data coupled with the protein pulldown data support a model where AQP2 phosphorylation mediates the 14-3-3 interaction. To examine whether any of the known phosphorylation sites in AQP2 may be involved, HEK293T cells (do not express AQP2) were co-transfected with wild-type AQP2 or various AQP2 phosphorylation deficient mutants (S256A, S261A, S264A, S269A) and HA-14-3-3θ and -ζ constructs. Cells were stimulated with forskolin followed by immunoprecipitation. In 14-3-3θ-transfected cells (Fig. 9*A*) and in samples immunoprecipitated with an HA antibody, AQP2 could not be detected in cells transfected with AQP2 S256A, and less AQP2 was observed in cells transfected with S264A or S269A. Conversely, in AQP2 IP samples, 14-3-3θ could not be detected in cells transfected with AQP2 S256A, and less 14-3-3 was detected in cells transfected with S264A or S269A. In 14-3-3ζ-transfected cells (Fig. 9*B*) and in samples immunoprecipitated with an HA antibody, AQP2 could not be detected in cells transfected with AQP2 S256A or S269A. Conversely, in AQP2 IP samples, 14-3-3ζ could not be detected in cells transfected with AQP2 S256A or S269A. These data suggest that Ser-256, Ser-264, and Ser-269 sites in AQP2 are important for the 14-3-3 interaction.

Direct Interaction of AQP2 Carboxyl-terminal Tail with 14-3-3—The potential for AQP2 to directly interact with 14-3-3 was studied using SPR. As demonstrated in Fig. 10*A*, a 44-amino acid peptide corresponding to the carboxyl-terminal

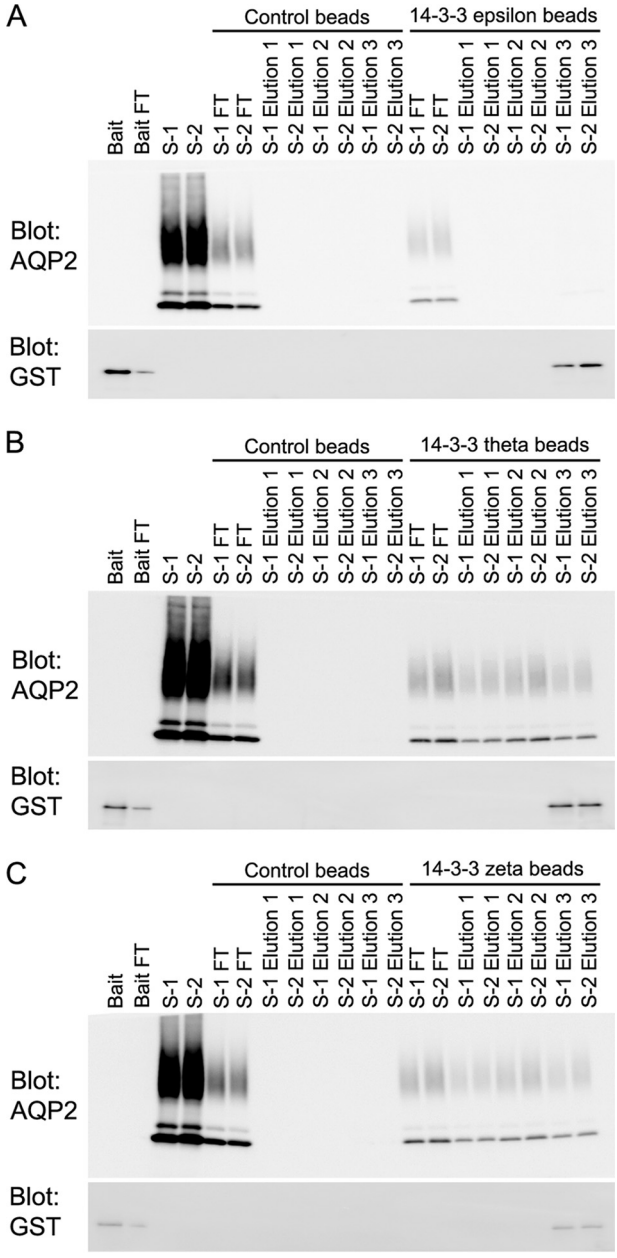

FIGURE 8. **GST pulldown assays using 14-3-3θ and -ζ and -ϵ.** GST pulldown assays were performed with dDAVP-treated mpkCCD$_{14}$ cell lysates as prey and GST-14-3-3ϵ, GST-14-3-3θ, or GST-14-3-3ζ as bait. Immunoblotting was performed using antibodies detecting total AQP2 or GST. Non-coated control beads or 14-3-3ϵ (*A*) coated beads displayed no interactions with AQP2, whereas AQP2 was consistently identified in eluates from either 14-3-3θ (*B*) or -ζ (*C*) coated beads. *S-1* and *S-2* represent different experimental samples. *FT* represents flow-through after binding of bait to beads or after incubation of beads with lysate prey. Elutions 1 and 2 are successive elutions with 10 mM glutathione, whereas elution 3 is a single elution using Laemmli sample buffer.

44 amino acids of AQP2 and phosphorylated at Ser-256 reproducibly associated with immobilized 14-3-3θ, with an apparent K_d of 0.5 μM. All other peptides (lacking Ser-256 phosphorylation) showed no significant interaction. 14-3-3 overlay assays (Fig. 10*B*) using 14-3-3ζ on immunoisolated AQP2 or the carboxyl-terminal peptides confirmed that a direct interaction, which was dependent on Ser-256 phosphorylation, was possible. In addition to the 14-3-3 signal at a molecular weight corresponding to AQP2, the presence of additional bands in AQP2 co-immunoprecipitation samples suggests that other proteins that associate with AQP2 may also interact with 14-3-3. Similar results were observed using 14-3-3θ during the overlay (not shown).

Stable Knockdown of 14-3-3θ and -ζ in mpkCCD$_{14}$ Cells Alters AQP2 Protein Abundances and Half-lives—To examine the role of 14-3-3θ and -ζ in regulation of AQP2, knockdown of each isoform individually in mpkCCD$_{14}$ cells using various 14-3-3 isoform-specific shRNA constructs was undertaken. Initial transient transfections were successful in identifying the most potent shRNAs for 14-3-3 knockdown (data not shown), which were subsequently used to generate stable knockdown mpkCCD$_{14}$ cells. Several independent cell populations were characterized by qRT-PCR (Fig. 11*A*) and Western blotting using isoform-selective antibodies (Fig. 11*B*). Line T1 and Z2 were utilized for subsequent studies. When grown on semipermeable supports for 10 days (dDAVP present for last 3 days), the T1 and Z2 cell lines showed no obvious morphological differences to control mpkCCD$_{14}$ cells and there were no significant differences in their transepithelial electrical resistances; control = 8845 $\pm$ 73 Ω/cm^2, T1 = 8845 $\pm$ 73 Ω/cm^2, Z1 = 8620 $\pm$ 173 Ω/cm^2. In total protein homogenates, AQP2 levels were significantly increased in T1 cells relative to control mpkCCD$_{14}$ cells, whereas in Z2 cells AQP2 levels were decreased by ~50% (Fig. 12*A*). No significant differences in the abundance of the V2R, or in AQP2 mRNA levels (qRT-PCR) between control, T1, or Z2 cell lines were detected (Fig. 13), suggesting that the effects of 14-3-3θ or -ζ knockdown were either on AQP2 translation efficiency or AQP2 degradation rate. To examine the latter, cycloheximide studies (inhibitor of protein translation) were performed in control, T1 and Z2 mpkCCD$_{14}$ cells (see "Experimental Procedures") and AQP2 protein levels were examined by immunoblotting (Fig. 12*C*). The calculated AQP2 protein half-life (Fig. 12*D*) in control mpkCCD$_{14}$ cells was 4.02 h (95% confidence interval 3.60 to 4.50), compared with 5.84 h (95% confidence interval 5.18 to 6.69) in T1 cells and 2.96 (95% confidence interval 2.66 to 3.34) h in Z2 cells, indicating that the altered AQP2 protein abundances in the various cell lines are partially due to significantly altered protein stability.

Stable Knockdown of 14-3-3θ and -ζ in mpkCCD$_{14}$ Cells Alters AQP2 Membrane Targeting, Phosphorylation, and Ubiquitylation—The abundance of AQP2 on the plasma membrane is regulated by a complex interplay between AQP2 phosphorylation and ubiquitylation. To examine a potential role of 14-3-3θ and -ζ in these mechanisms the plasma membrane abundance, ubiquitylation, and phosphorylation status of AQP2 in the various mpkCCD$_{14}$ cell lines was examined. To mimic a physiological setting, cells were examined under control, acute dDAVP stimulated, or acute dDAVP stimulated followed by dDAVP washout conditions. Representative immunoblotting data are shown in Fig. 14*A*. In control mpkCCD$_{14}$ cells, the abundance of AQP2 on the apical plasma membrane significantly increased following 20 min of dDAVP treatment, followed by a reduction 30 min after dDAVP washout (Fig. 14*B*). A similar pattern of AQP2 distribution was observed in T1 cells, however, the plasma membrane levels of AQP2 follow-

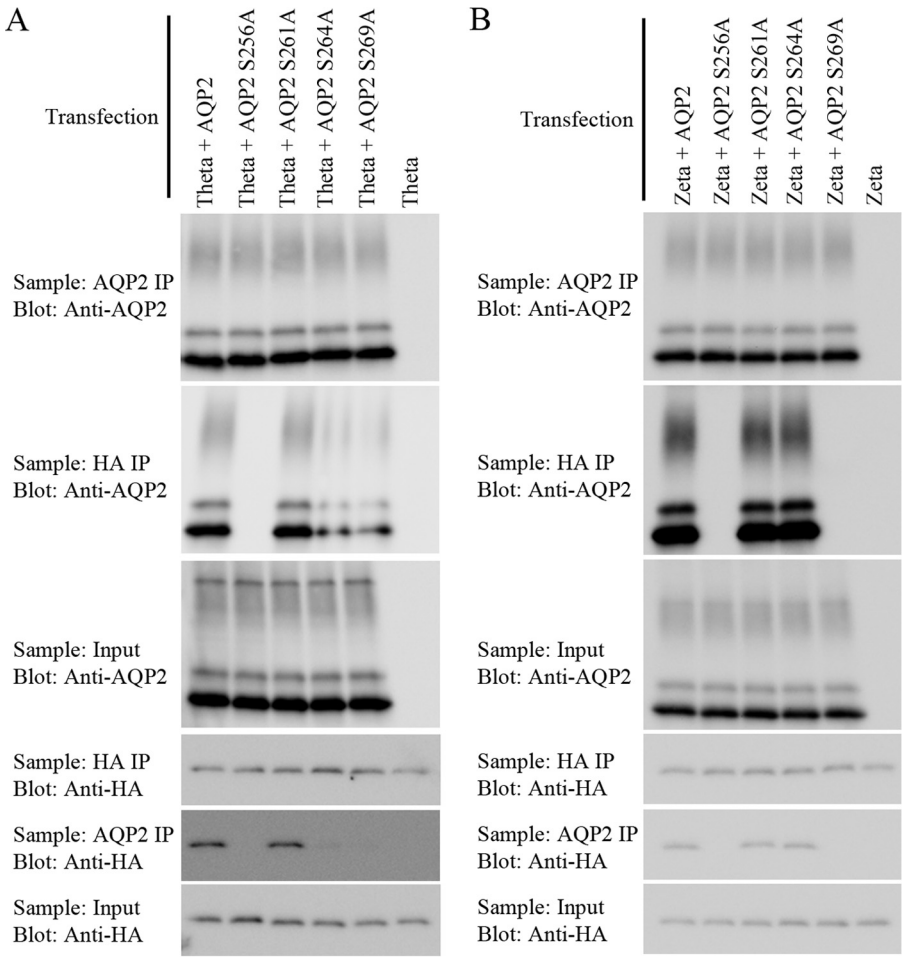

FIGURE 9. **Phosphorylation of AQP2 at Ser-256 is critical for 14-3-3 interactions.** HEK293T cells were co-transfected with wild-type AQP2 or various AQP2 phosphorylation deficient mutants (S256A, S261A, S264A, and S269A) and HA-14-3-3θ or -ζ constructs. *A*, in 14-3-3θ-transfected cells, in HA IP samples AQP2 could not be detected in cells transfected with AQP2 S256A, and less AQP2 was observed in cells transfected with S264A or S269A. Conversely, in AQP2 IP samples, 14-3-3θ could not be detected in cells transfected with AQP2 S256A, and less 14-3-3 was detected in cells transfected with S264A or S269A. *B*, in 14-3-3ζ-transfected cells, in HA IP samples AQP2 could not be detected in cells transfected with AQP2 S256A or S269A. Conversely, in AQP2 IP samples, 14-3-3ζ could not be detected in cells transfected with AQP2 S256A or S269A.

ing dDAVP stimulation were significantly higher than in control mpkCCD$_{14}$ cells (Fig. 14, *B* and *C*). Although AQP2 redistribution in Z2 cells followed a similar trend as in control and T1 mpkCCD$_{14}$ cells (Fig. 14, *B* and *C*), the AQP2 plasma membrane abundances were not significantly different under any of the examined conditions. Under identical conditions, ubiquitylated AQP2 levels in all 3 cell lines were significantly enhanced during dDAVP and dDAVP washout conditions (Fig. 14*D*). Furthermore, ubiquitylated AQP2 levels were ~2-fold higher in Z2 cells compared with control and T1 mpkCCD$_{14}$ cells (Fig. 14*E*), providing an explanation for the decreased AQP2 protein half-life in these cells (Fig. 12). Similarly to previous observations (Fig. 6), in all 3 cell lines Ser(P)-269 AQP2 levels in total cell lysates were significantly increased after acute dDAVP treatment, but were reduced following dDAVP washout (Fig. 14*F*). The levels of Ser(P)-269 levels following dDAVP treatment were significantly higher in T1 cells relative to dDAVP-treated mpkCCD$_{14}$ cells (Fig. 14*G*), matching the greater AQP2 plasma membrane abundance under similar conditions. Although Ser(P)-269 AQP2 levels were consistently reduced in the Z2 cells, these did not reach significance (Fig. 14*G*).

Discussion

The water channel AQP2 is the AVP-regulated water channel of the kidney principal cells. AQP2 function is highly dependent on its phosphorylation status, which mediates various phosphorylation-dependent AQP2 protein/protein interactions (29). In this study we examined the hypothesis that 14-3-3 proteins, which often interact with phosphorylated proteins, can modulate the function of AQP2.

All 14-3-3 isoforms, except σ, were detected in mouse kidney and mpkCCD$_{14}$ cells. The absence of σ corresponds with recent large scale RNA sequencing studies of isolated kidney segments from rat (12) or cDNA arrays of isolated rat IMCD (39). Although redundancy among 14-3-3 isoforms has been debated (40), 14-3-3ϵ, -β, -η, and -ζ had distinct distributions in mouse IMCD cells, suggesting that different isoforms fulfill different roles in these cells. In particular, the 14-3-3ζ isoform, whose distribution was similar to AQP2, is ideally placed to play a role in AQP2 regulation. Although limited to the resolution of confocal microscopy, the punctate distribution of ζ at the apical plasma membrane is similar to that observed for AQP2 under

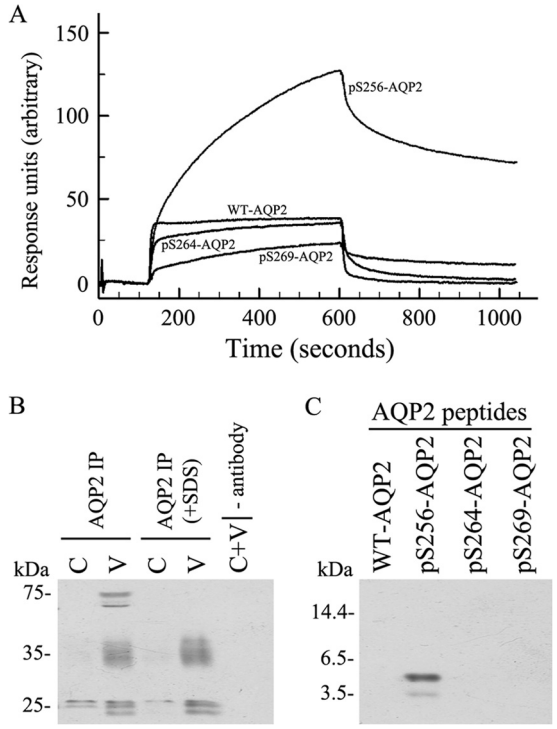

FIGURE 10. **The carboxyl-terminal tail of AQP2 can interact directly with 14-3-3.** *A,* SPR analysis of 14-3-3θ with various polypeptides corresponding to the carboxyl-terminal 44 amino acids of AQP2. The *y* axis indicates the difference between the sample and control runs in relative response units. A Ser-256 phosphorylated AQP2 peptide (*pS256-AQP2*) reproducibly associated with immobilized 14-3-3θ, with a K_d of 0.5 μM. *B,* 14-3-3ζ overlay assays on immunoisolated AQP2 under control (*C*) or acute dDAVP (*V*) conditions. +*SDS* indicates lysates were treated with 1% SDS before immunoisolation (see "Experimental Procedures"). *C,* similar overlay assay on AQP2 carboxyl-terminal peptides confirmed the dependence of Ser256 phosphorylation for the AQP2/14-3-3 interaction.

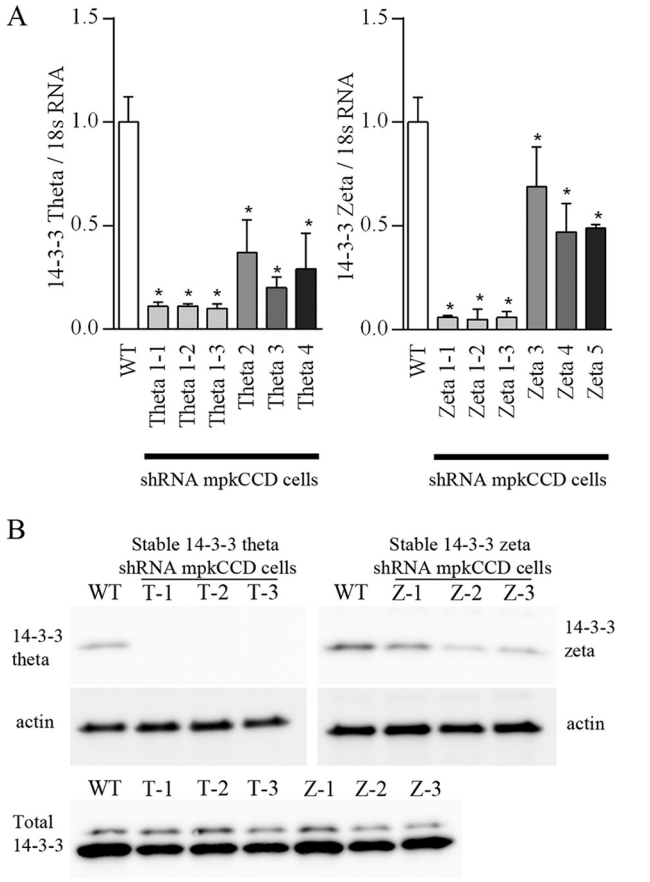

FIGURE 11. **Characterization of mpkCCD$_{14}$ cells with stable knockdown of 14-3-3θ and -ζ.** Lentivirus-mediated delivery of 14-3-3θ and -ζ shRNAs was used to generate stable knockdown of individual isoforms in mpkCCD$_{14}$ cells. *A,* qRT-PCR analysis of mRNA levels of 14-3-3θ or -ζ in control (WT) or 6 independent cell populations. *B,* Western blotting using isoform-selective antibodies on the 3 independent cell populations with the lowest 14-3-3 mRNA levels. * indicates $p < 0.05$ relative to the WT cells.

certain conditions (24), where a proportion of AQP2 is located in "endocytosis-resistant" membrane domains after AVP treatment (41).

Selective alterations in 14-3-3 isoform expression by AVP further indicated a link between AQP2 function and 14-3-3 proteins. AQP2 is an AVP-induced protein *in vivo*, with AVP increasing AQP2 abundance via stimulating AQP2 gene transcription (42). In mpkCCD$_{14}$ cells, similarly to AQP2, 14-3-3β and -ζ were increased in expression following long-term dDAVP stimulation, whereas η and θ expression levels were decreased. An increase in ζ expression in IMCD cells following long-term dDAVP treatment of rats has been observed previously (43). The finding that dDAVP increased 14-3-3β levels fits well with the known role of AVP to increase collecting duct NaCl transport (reviewed in Ref. 44). In principle, increased 14-3-3β would enhance the known 14-3-3β interaction with Nedd4-2, thereby inhibiting Nedd4-2-mediated ENaC ubiquitylation and ultimately increasing sodium transport (15, 18, 45).

The data collected from immunoprecipitation studies using mpkCCD$_{14}$ and HEK cells, combined with the results from GST pulldown assays strongly infers that AQP2 interacts with 14-3-3θ and -ζ. Furthermore, these selective 14-3-3 interactions being phosphorylation-dependent are supported by 1) an increased interaction of AQP2 with 14-3-3 following dDAVP treatment in a time scale where AQP2 phosphorylation is known to occur; 2) phosphatase inhibitors potentiating the dDAVP-induced AQP2/14-3-3 interactions; 3) a loss of AQP2 in GST pulldowns following λ-phosphatase treatment of prey lysates; 4) reduced AQP2/14-3-3 interactions in various AQP2 phosphorylation-deficient mutants; and 5) direct interaction of only Ser(P)-256 peptides with immobilized 14-3-3. Overlay assays and SPR analysis provided evidence that a direct 14-3-3/AQP2 interaction was possible, which was critically dependent on Ser-256 phosphorylation. However, as 14-3-3 is known to associate with other proteins that can interact with AQP2, *e.g.* AKAP, Nedd4-2, Hsp70, BiP, β-actin, tropomyosin, PKA, and PP1 (46–48), we cannot rule out that other proteins are involved in, or possibly stabilize the interaction, as part of a multiprotein complex. Interestingly, the interaction of AQP2 with 14-3-3θ and -ζ differs to other 14-3-3 membrane protein interactions observed in the kidney, *e.g.* the sodium hydrogen exchanger NHE1 association with 14-3-3β (49) and the UT-A urea transporter association with 14-3-3γ (13), providing additional evidence that 14-3-3 isoforms are not redundant but rather play selective roles in modulating protein function.

Lentiviral mediated delivery of 14-3-3θ or -ζ shRNA constructs to mpkCCD$_{14}$ cells uncovered selective, but complex, roles of these isoforms in modulating AQP2 function. Knock-

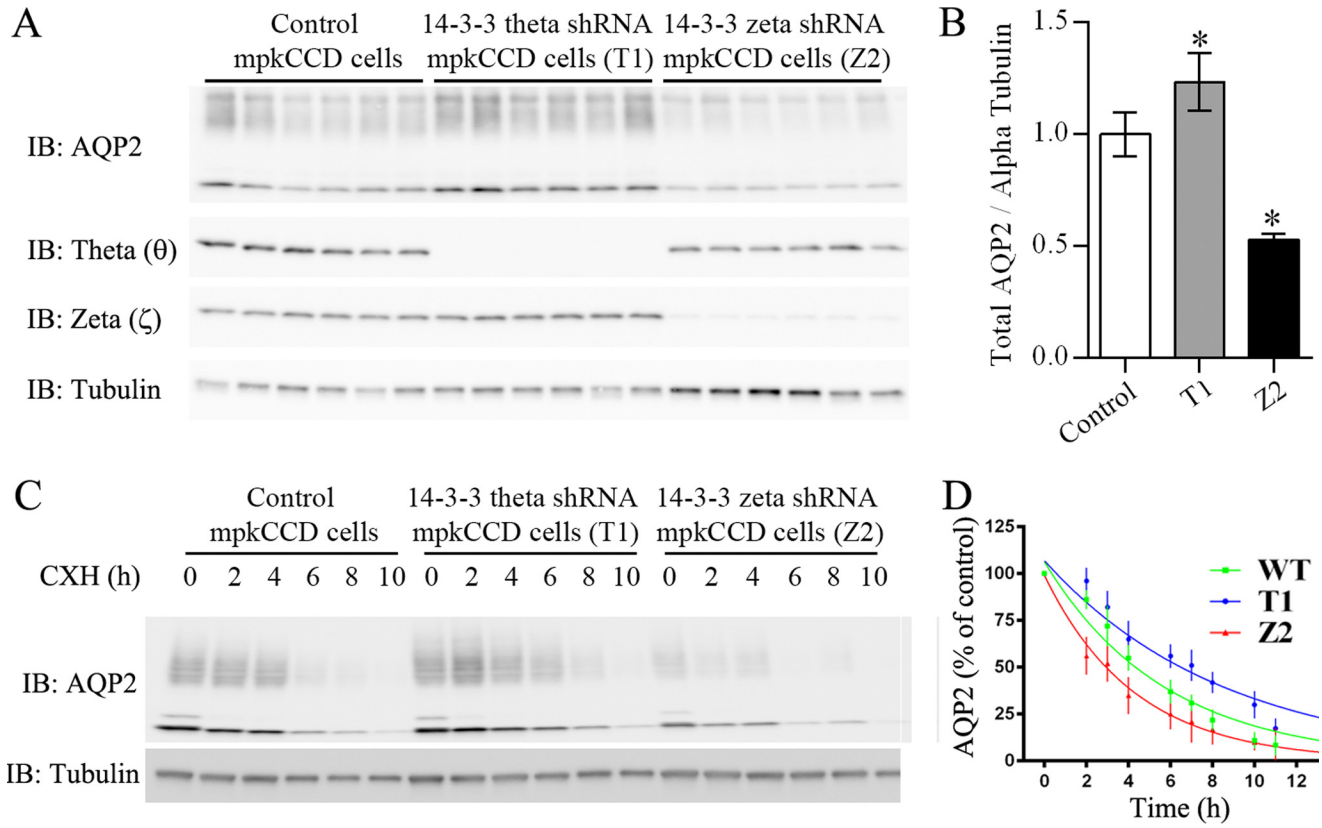

FIGURE 12. **Stable knockdown of 14-3-3θ and -ζ in mpkCCD$_{14}$ cells alters AQP2 protein abundances and half-life.** *A,* representative immunoblots (*IB*) of AQP2, 14-3-3θ, 14-3-3ζ, and α-tubulin abundances in protein lysates from control mpkCCD$_{14}$ cells or cells with stable knockdown of 14-3-3θ or -ζ. Each *lane* represents a different sample. *B,* summary quantification data of AQP2 abundance. * indicates $p < 0.05$ relative to the control cells. *C,* representative immunoblotting of AQP2 and α-tubulin in a cycloheximide (*CHX*) chase experiment. Elevated and prolonged AQP2 protein levels were consistently observed in the θ knockdown mpkCCD$_{14}$ cells, whereas they were reduced rapidly in the ζ knockdown cells. *D,* curves show summarized cycloheximide data fitted using nonlinear regression and a one-phase exponential decay equation. AQP2 abundance is normalized to zero time point. Values are obtained from 4 independent experiments with $n = 3–6$ for each individual time point.

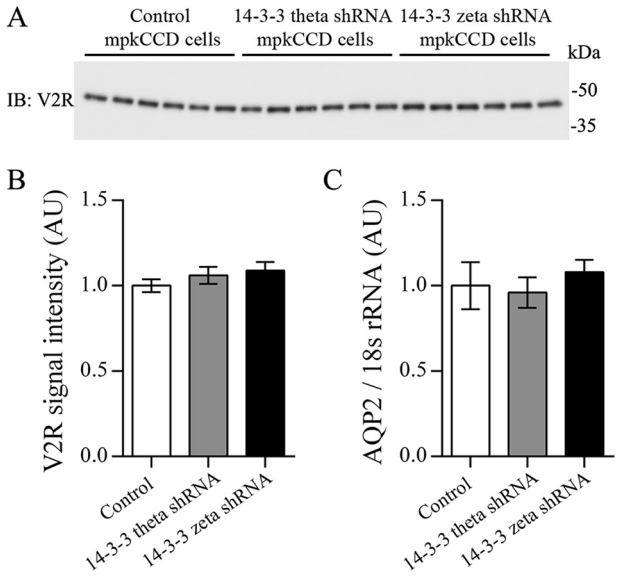

FIGURE 13. **Analysis of V2R protein and AQP2 mRNA levels in T1 and Z2 cell lines.** *A,* protein abundance of the V2R was assessed by immunoblotting of total protein homogenates from the 14-3-3θ (*T1*) and 14-3-3ζ (*Z2*) knockdown cell lines. *B,* no significant differences were detected in the abundance of the V2R. *C,* no significant differences were detected in AQP2 mRNA levels between control, T1 or Z2 cell lines.

down of 14-3-3ζ resulted in increased AQP2 ubiquitylation, decreased AQP2 half-life, and ultimately drastically reduced AQP2 levels. These data suggest that 14-3-3ζ "protects" AQP2 from being ubiquitylated and directed into the degradation pathway. The distinct localization of 14-3-3ζ suggests that this "protection" occurs in the apical plasma membrane domain, where otherwise ubiquitylation of AQP2 followed by endocytic retrieval and subsequent degradation is initiated (30). What potential mechanisms could be behind such a response? Previous studies from our group and others have shown that AVP-induced phosphorylation of AQP2 at Ser-256 and Ser-269 mediates AQP2 membrane accumulation by decreasing the rate of AQP2 internalization, a process that ultimately results in increased AQP2 protein half-life (23, 29). Therefore, it is interesting to speculate one model (Fig. 15) where: 1) upon AVP stimulation AQP2 undergoes phosphorylation at Ser-256 that facilitates its trafficking to the plasma membrane; 2) at the membrane AQP2 undergoes Ser-269 phosphorylation; 3) the individual or combined effect of the two AQP2 phosphorylation events mediates an interaction with 14-3-3ζ; and 4) the AQP2·14-3-3ζ complex prevents or limits binding of an unknown E3 ligase or an adapter protein to AQP2 thus reducing AQP2 ubiquitylation, internalization, and subsequent degradation. In line with this mechanism, mutation of AQP2 at Ser-256 or Ser-269 to alanine resulted in the complete absence, or dramatically reduced interaction of AQP2 with 14-3-3ζ, respectively. Furthermore, AQP2 membrane abundance and Ser-269 phosphorylation were reduced in the 14-3-3ζ knockdown cells, suggesting a higher rate of internalization. Finally,

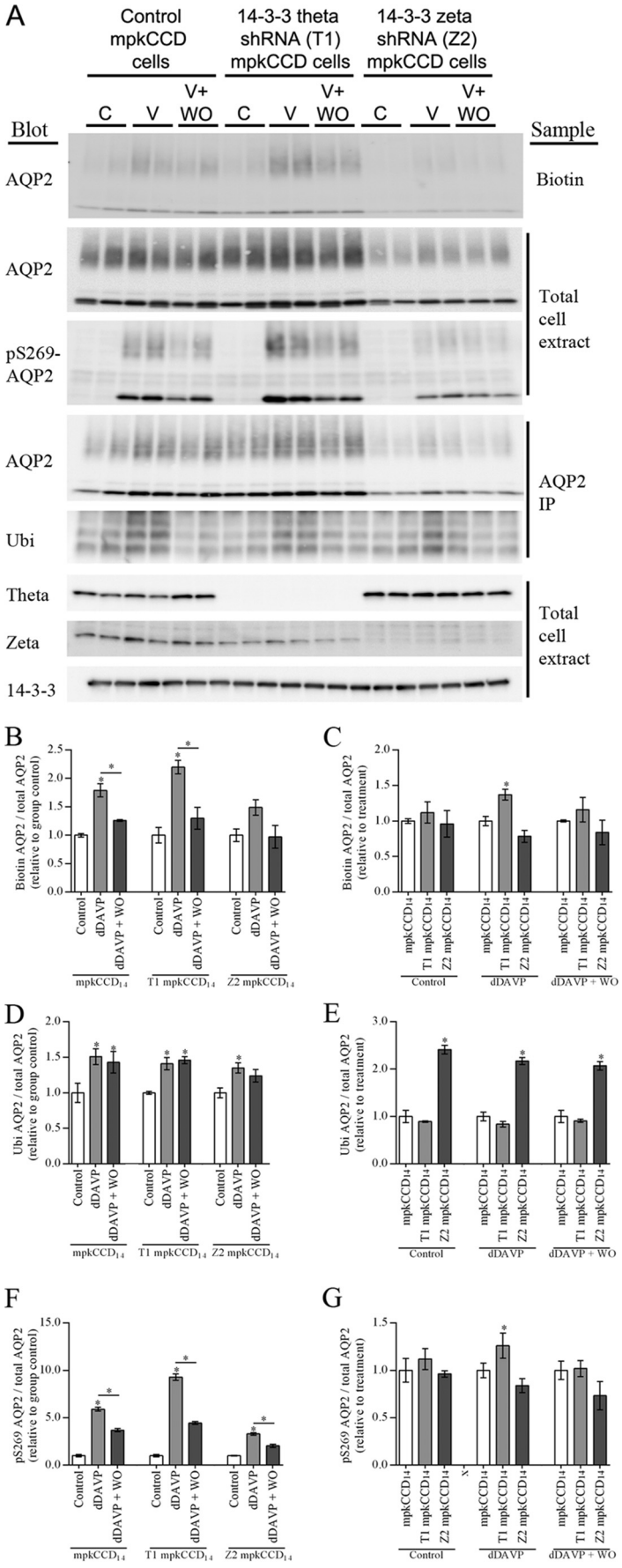
A
Control mpkCCD cells
14-3-3 theta shRNA (T1) mpkCCD cells
14-3-3 zeta shRNA (Z2) mpkCCD cells
C V V+ WO C V V+ WO C V V+ WO
Blot
Sample
AQP2
Biotin
AQP2
pS269-AQP2
Total cell extract
AQP2
Ubi
AQP2 IP
Theta
Zeta
14-3-3
Total cell extract
B
Biotin AQP2 / total AQP2 (relative to group control)
Control
dDAVP
dDAVP + WO
mpkCCD14
T1 mpkCCD14
Z2 mpkCCD14
C
Biotin AQP2 / total AQP2 (relative to treatment)
Control
dDAVP
dDAVP + WO
D
Ubi AQP2 / total AQP2 (relative to group control)
E
Ubi AQP2 / total AQP2 (relative to treatment)
F
pS269 AQP2 / total AQP2 (relative to group control)
G
pS269 AQP2 / total AQP2 (relative to treatment)

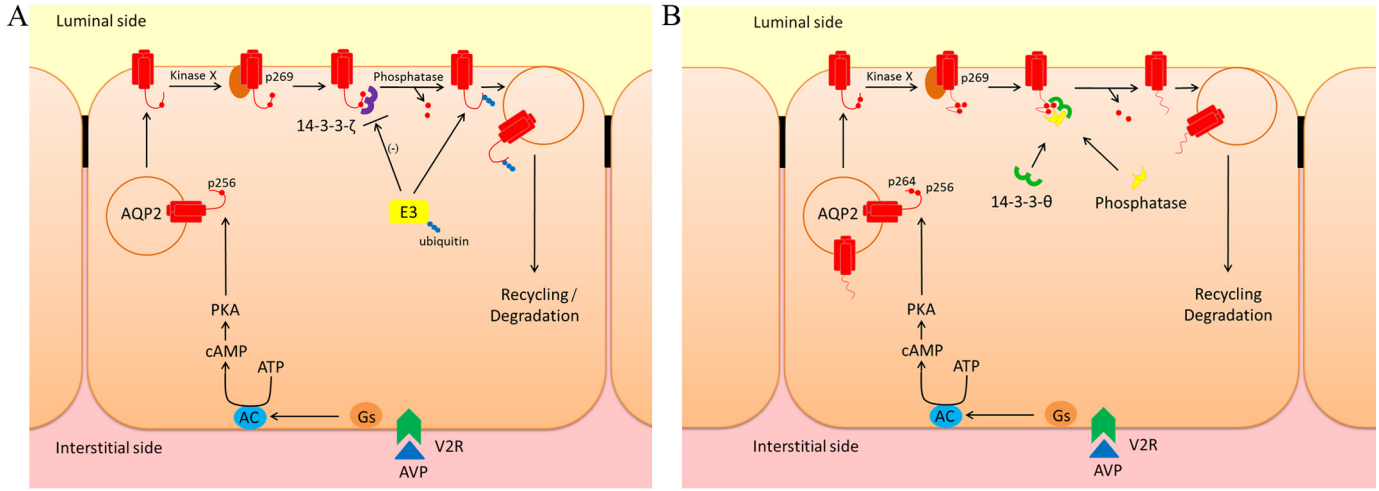

FIGURE 15. **Proposed models for 14-3-3 regulation of AQP2.** *A,* upon AVP stimulation AQP2 undergoes phosphorylation at Ser-256 that facilitates its trafficking to the plasma membrane. At the membrane AQP2 undergoes Ser-269 phosphorylation. The individual or combined effect of the two AQP2 phosphorylation events mediates an interaction with 14-3-3ζ. The AQP2·14-3-3ζ complex prevents or limits binding of an unknown E3 ligase or an adapter protein to AQP2 thus reducing AQP2 ubiquitylation, internalization, and subsequent degradation. *B,* upon AVP stimulation AQP2 undergoes phosphorylation at Ser-256 (and possibly Ser-264) that facilitates its trafficking to the plasma membrane. At the membrane, AQP2 undergoes Ser-269 phosphorylation. The individual or combined effect of the three AQP2 phosphorylation events mediates an interaction with 14-3-3θ, which recruits a protein phosphatase to AQP2 resulting in dephosphorylation and internalization.

the dDAVP-induced increases in 14-3-3ζ abundance observed in mpkCCD$_{14}$ cells support a role for 14-3-3ζ in reducing the degree of AQP2 degradation during long-term AVP stimulation, thus aiding in the conservation of body water.

A simple model for the role of 14-3-3θ in AQP2 regulation is less obvious. Conversely to the effects of 14-3-3ζ, knockdown of 14-3-3θ resulted in significantly greater AQP2 abundance; a result of increased AQP2 protein half-life. Surprisingly, although AQP2 ubiquitylation levels in the 14-3-3ζ knockdown mpkCCD$_{14}$ cells were marginally decreased relative to control, these effects were not significant; suggesting the possibility of non-ubiquitin-dependent AQP2 degradation. Further studies are required to examine this possibility. Despite no significant reductions in AQP2 ubiquitylation levels, AQP2 levels on the plasma membrane were significantly enhanced after dDAVP treatment, accompanied by higher levels of pS269 AQP2. This data points toward 14-3-3θ recruiting/stabilizing a protein phosphatase complex that specifically targets the Ser(P)-269 site of AQP2. Attractive possibilities are protein phosphatases 1 and 2A, which can dephosphorylate Ser(P)-269 AQP2 (23), and can also interact with 14-3-3 proteins (47, 48). The possibility of 14-3-3θ interacting with Ser(P)-269 is supported by the reduced interaction of AQP2 S269A with 14-3-3θ in HEK293 cells. Furthermore, our previous studies have indicated a unique role for Ser(P)-269 AQP2 in reducing AQP2 endocytosis despite no alterations in AQP2 ubiquitylation levels (23). This "negative" modulatory role of 14-3-3θ for AQP2 is supported by the decreased θ levels observed in mpkCCD$_{14}$ cells following long-term dDAVP treatment.

What is the physiological role of the 14-3-3/AQP2 interaction? Vasopressin stimulation of various animal models induces phosphorylation of AQP2 at Ser-256, Ser-264, and Ser-269, with Ser-256 phosphorylation acting as a "master switch" that is needed for the subsequent downstream phosphorylation of AQP2 (21). Although the exact role of each of these phosphorylation sites in isolation is still not completely clear, the Ser-256 site is critical for vasopressin-stimulated accumulation of AQP2 on the plasma membrane and for the AQP2/14-3-3 interactions. This suggests that the interactions occur downstream of vasopressin signaling and, based on the localization of the different isoforms, potentially even in alternative subcellular compartments. Whether a different pool of AQP2 binds at any one time to 14-3-3ζ/θ, resulting in both positive/negative effects on AQP2 membrane abundance and function is not known. However, it is likely that the dual 14-3-3 interactions act in concert to fine-tune the amount of AQP2 on the plasma membrane and help modulate the degree of water reabsorption by the principal cell.

In conclusion, we have determined that an AVP-regulated and phosphorylation-dependent interaction occurs between AQP2 and 14-3-3θ and -ζ. These interactions play a divergent role in modulating AQP2 trafficking, phosphorylation, ubiquitylation, and degradation. Our studies confirm that AQP2 function is highly dependent on phosphorylation-dependent protein interactions with its carboxyl-terminal domain and furthermore, provide additional evidence that various isoforms of 14-3-3 play divergent roles in the cell.

FIGURE 14. **Stable knockdown of 14-3-3θ and -ζ in mpkCCD$_{14}$ cells alters AQP2 membrane targeting, phosphorylation, and ubiquitylation.** The three mpkCCD$_{14}$ cell lines under control (*C*), acute dDAVP stimulated (*V*), or acute dDAVP stimulated followed by dDAVP washout (*V + WO*) conditions were assessed for AQP2 membrane abundance via biotinylation, alongside analysis of AQP2 phosphorylation levels and ubiquitylation status. *A,* representative immunoblotting data of AQP2, pS269-AQP2, ubiquitin, total 14-3-3, 14-3-3θ, and 14-3-3ζ levels in the various fractions. *B* and *C,* summary quantification data for biotinylated AQP2. *D* and *E,* summary quantification data for ubiquitylated AQP2. *F* and *G,* summary quantification data for pS269-AQP2. Each paired graph represents data normalized and analyzed in two different ways to facilitate comparisons between the experimental conditions within an individual cell line, or between individual cells lines for each experimental condition. * indicates $p < 0.05$ relative to the control condition/cell line, or from the group as indicated.

Author Contributions—R. A. F. conceived the study. H. B. M.O., J. E. S. H., T. A., M. A., N. M., M. T., S. K. M., and R. A. F. performed the study. V. B. provided essential reagents and helped on study design. H. B. M. O. and R. A. F. drafted the manuscript. All authors read and approved the final manuscript.

Acknowledgments—Tina Drejer, Inger-Merete Paulsen, Christian Westberg, Ahmed Basim Abduljabar, Helle Høyer, and Anne Marie Bundsgaard are thanked for expert technical assistance. Michele Tinti, Gavuthami Murugesan, and Carol MacKintosh are thanked for helpful discussions on identifying 14-3-3 interaction motifs and overlay assay conditions.

References

1. Mackintosh, C. (2004) Dynamic interactions between 14-3-3 proteins and phosphoproteins regulate diverse cellular processes. *Biochem. J.* **381,** 329–342
2. Fu, H., Subramanian, R. R., and Masters, S. C. (2000) 14-3-3 proteins: structure, function, and regulation. *Annu. Rev. Pharmacol. Toxicol.* **40,** 617–647
3. Morrison, D. K. (2009) The 14-3-3 proteins: integrators of diverse signaling cues that impact cell fate and cancer development. *Trends Cell Biol.* **19,** 16–23
4. Muslin, A. J., Tanner, J. W., Allen, P. M., and Shaw, A. S. (1996) Interaction of 14-3-3 with signaling proteins is mediated by the recognition of phosphoserine. *Cell* **84,** 889–897
5. Johnson, C., Crowther, S., Stafford, M. J., Campbell, D. G., Toth, R., and MacKintosh, C. (2010) Bioinformatic and experimental survey of 14-3-3-binding sites. *Biochem. J.* **427,** 69–78
6. Aitken, A. (2011) Post-translational modification of 14-3-3 isoforms and regulation of cellular function. *Semin. Cell Dev. Biol.* **22,** 673–680
7. Bridges, D., and Moorhead, G. B. (2005) 14-3-3 proteins: a number of functions for a numbered protein. *Science's STKE* **2005,** re10
8. Dougherty, M. K., and Morrison, D. K. (2004) Unlocking the code of 14-3-3. *J. Cell Sci.* **117,** 1875–1884
9. Wilker, E., and Yaffe, M. B. (2004) 14-3-3 proteins: a focus on cancer and human disease. *J. Mol. Cell. Cardiol.* **37,** 633–642
10. Pozuelo Rubio, M., Geraghty, K. M., Wong, B. H., Wood, N. T., Campbell, D. G., Morrice, N., and Mackintosh, C. (2004) 14-3-3-affinity purification of over 200 human phosphoproteins reveals new links to regulation of cellular metabolism, proliferation and trafficking. *Biochem. J.* **379,** 395–408
11. Liang, S., Xu, Y., Shen, G., Liu, Q., Zhao, X., Xu, Z., Xie, X., Gong, F., Li, R., and Wei, Y. (2009) Quantitative protein expression profiling of 14-3-3 isoforms in human renal carcinoma shows 14-3-3 epsilon is involved in limitedly increasing renal cell proliferation. *Electrophoresis* **30,** 4152–4162
12. Lee, J. W., Chou, C. L., and Knepper, M. A. (2015) Deep sequencing in microdissected renal tubules identifies nephron segment-specific transcriptomes. *J. Am. Soc. Nephrol.* **26,** 2669–2677
13. Feng, X., Li, Z., Du, Y., Fu, H., Klein, J. D., Cai, H., Sands, J. M., and Chen, G. (2015) Downregulation of urea transporter UT-A1 activity by 14-3-3 protein. *Am. J. Physiol. Renal Physiol.* **309,** F71–F78
14. Bhalla, V., Daidié, D., Li, H., Pao, A. C., LaGrange, L. P., Wang, J., Vandewalle, A., Stockand, J. D., Staub, O., and Pearce, D. (2005) Serum- and glucocorticoid-regulated kinase 1 regulates ubiquitin ligase neural precursor cell-expressed, developmentally down-regulated protein 4-2 by inducing interaction with 14-3-3. *Mol. Endocrinol.* **19,** 3073–3084
15. Staub, O., Gautschi, I., Ishikawa, T., Breitschopf, K., Ciechanover, A., Schild, L., and Rotin, D. (1997) Regulation of stability and function of the epithelial Na^+ channel (ENaC) by ubiquitination. *EMBO J.* **16,** 6325–6336
16. Chandran, S., Li, H., Dong, W., Krasinska, K., Adams, C., Alexandrova, L., Chien, A., Hallows, K. R., and Bhalla, V. (2011) Neural precursor cell-expressed developmentally down-regulated protein 4-2 (Nedd4-2) regulation by 14-3-3 protein binding at canonical serum and glucocorticoid kinase 1 (SGK1) phosphorylation sites. *J. Biol. Chem.* **286,** 37830–37840
17. Ichimura, T., Yamamura, H., Sasamoto, K., Tominaga, Y., Taoka, M., Kakiuchi, K., Shinkawa, T., Takahashi, N., Shimada, S., and Isobe, T. (2005) 14-3-3 proteins modulate the expression of epithelial Na^+ channels by phosphorylation-dependent interaction with Nedd4-2 ubiquitin ligase. *J. Biol. Chem.* **280,** 13187–13194
18. Liang, X., Butterworth, M. B., Peters, K. W., Walker, W. H., and Frizzell, R. A. (2008) An obligatory heterodimer of 14-3-3β and 14-3-3ϵ is required for aldosterone regulation of the epithelial sodium channel. *J. Biol. Chem.* **283,** 27418–27425
19. Barile, M., Pisitkun, T., Yu, M. J., Chou, C. L., Verbalis, M. J., Shen, R. F., and Knepper, M. A. (2005) Large scale protein identification in intracellular aquaporin-2 vesicles from renal inner medullary collecting duct. *Mol. Cell Proteomics* **4,** 1095–1106
20. Moeller, H. B., and Fenton, R. A. (2012) Cell biology of vasopressin-regulated aquaporin-2 trafficking. *Pflugers Arch.* **464,** 133–144
21. Hoffert, J. D., Fenton, R. A., Moeller, H. B., Simons, B., Tchapyjnikov, D., McDill, B. W., Yu, M. J., Pisitkun, T., Chen, F., and Knepper, M. A. (2008) Vasopressin-stimulated increase in phosphorylation at Ser-269 potentiates plasma membrane retention of aquaporin-2. *J. Biol. Chem.* **283,** 24617–24627
22. Hoffert, J. D., Pisitkun, T., Wang, G., Shen, R. F., and Knepper, M. A. (2006) Quantitative phosphoproteomics of vasopressin-sensitive renal cells: regulation of aquaporin-2 phosphorylation at two sites. *Proc. Natl. Acad. Sci. U.S.A.* **103,** 7159–7164
23. Moeller, H. B., Aroankins, T. S., Slengerik-Hansen, J., Pisitkun, T., and Fenton, R. A. (2014) Phosphorylation and ubiquitylation are opposing players in regulating endocytosis of the water channel aquaporin-2. *J. Cell Sci.* **127,** 3174–3183
24. Moeller, H. B., Knepper, M. A., and Fenton, R. A. (2009) Serine 269 phosphorylated aquaporin-2 is targeted to the apical membrane of collecting duct principal cells. *Kidney Int.* **75,** 295–303
25. Hoffert, J. D., Nielsen, J., Yu, M. J., Pisitkun, T., Schleicher, S. M., Nielsen, S., and Knepper, M. A. (2007) Dynamics of aquaporin-2 serine-261 phosphorylation in response to short-term vasopressin treatment in collecting duct. *Am. J. Physiol. Renal Physiol.* **292,** F691–F700
26. Fenton, R. A., Moeller, H. B., Hoffert, J. D., Yu, M. J., Nielsen, S., and Knepper, M. A. (2008) Acute regulation of aquaporin-2 phosphorylation at Ser-264 by vasopressin. *Proc. Natl. Acad. Sci. U.S.A.* **105,** 3134–3139
27. Rice, W. L., Zhang, Y., Chen, Y., Matsuzaki, T., Brown, D., and Lu, H. A. (2012) Differential, phosphorylation dependent trafficking of AQP2 in LLC-PK1 cells. *PloS One* **7,** e32843
28. van Balkom, B. W., Savelkoul, P. J., Markovich, D., Hofman, E., Nielsen, S., van der Sluijs, P., and Deen, P. M. (2002) The role of putative phosphorylation sites in the targeting and shuttling of the aquaporin-2 water channel. *J. Biol. Chem.* **277,** 41473–41479
29. Moeller, H. B., Praetorius, J., Rützler, M. R., and Fenton, R. A. (2010) Phosphorylation of aquaporin-2 regulates its endocytosis and protein-protein interactions. *Proc. Natl. Acad. Sci. U.S.A.* **107,** 424–429
30. Kamsteeg, E. J., Hendriks, G., Boone, M., Konings, I. B., Oorschot, V., van der Sluijs, P., Klumperman, J., and Deen, P. M. (2006) Short-chain ubiquitination mediates the regulated endocytosis of the aquaporin-2 water channel. *Proc. Natl. Acad. Sci. U.S.A.* **103,** 18344–18349
31. Fenton, R. A., Brønd, L., Nielsen, S., and Praetorius, J. (2007) Cellular and subcellular distribution of the type-2 vasopressin receptor in the kidney. *Am. J. Physiol. Renal Physiol.* **293,** F748–760
32. Yu, M. J., Miller, R. L., Uawithya, P., Rinschen, M. M., Khositseth, S., Braucht, D. W., Chou, C. L., Pisitkun, T., Nelson, R. D., and Knepper, M. A. (2009) Systems-level analysis of cell-specific AQP2 gene expression in renal collecting duct. *Proc. Natl. Acad. Sci. U.S.A.* **106,** 2441–2446
33. Loo, C. S., Chen, C. W., Wang, P. J., Chen, P. Y., Lin, S. Y., Khoo, K. H., Fenton, R. A., Knepper, M. A., and Yu, M. J. (2013) Quantitative apical membrane proteomics reveals vasopressin-induced actin dynamics in collecting duct cells. *Proc. Natl. Acad. Sci. U.S.A.* **110,** 17119–17124
34. Tamma, G., Lasorsa, D., Ranieri, M., Mastrofrancesco, L., Valenti, G., and Svelto, M. (2011) Integrin signaling modulates AQP2 trafficking via Arg-Gly-Asp (RGD) motif. *Cell. Physiol. Biochem.* **27,** 739–748
35. Kristiansen, M., Graversen, J. H., Jacobsen, C., Sonne, O., Hoffman, H. J.,

Law, S. K., and Moestrup, S. K. (2001) Identification of the haemoglobin scavenger receptor. *Nature* **409,** 198–201
36. Panni, S., Montecchi-Palazzi, L., Kiemer, L., Cabibbo, A., Paoluzi, S., Santonico, E., Landgraf, C., Volkmer-Engert, R., Bachi, A., Castagnoli, L., and Cesareni, G. (2011) Combining peptide recognition specificity and context information for the prediction of the 14-3-3-mediated interactome in *S. cerevisiae* and *H. sapiens*. *Proteomics* **11,** 128–143
37. Tinti, M., Johnson, C., Toth, R., Ferrier, D. E., and Mackintosh, C. (2012) Evolution of signal multiplexing by 14-3-3-binding 2R-ohnologue protein families in the vertebrates. *Open Biol.* **2,** 120103
38. Madeira, F., Tinti, M., Murugesan, G., Berrett, E., Stafford, M., Toth, R., Cole, C., MacKintosh, C., and Barton, G. J. (2015) 14-3-3-Pred: improved methods to predict 14-3-3-binding phosphopeptides. *Bioinformatics* **31,** 2276–2283
39. Uawithya, P., Pisitkun, T., Ruttenberg, B. E., and Knepper, M. A. (2008) Transcriptional profiling of native inner medullary collecting duct cells from rat kidney. *Physiol. Genomics* **32,** 229–253
40. Paul, A. L., Denison, F. C., Schultz, E. R., Zupanska, A. K., and Ferl, R. J. (2012) 14-3-3 phosphoprotein interaction networks: does isoform diversity present functional interaction specification? *Front. Plant Sci.* **3,** 190
41. Bouley, R., Hawthorn, G., Russo, L. M., Lin, H. Y., Ausiello, D. A., and Brown, D. (2006) Aquaporin 2 (AQP2) and vasopressin type 2 receptor (V2R) endocytosis in kidney epithelial cells: AQP2 is located in "endocytosis-resistant" membrane domains after vasopressin treatment. *Biol. Cell* **98,** 215–232
42. Kortenoeven, M. L., Trimpert, C., van den Brand, M., Li, Y., Wetzels, J. F., and Deen, P. M. (2012) In mpkCCD cells, long-term regulation of aquaporin-2 by vasopressin occurs independent of protein kinase A and CREB but may involve Epac. *Am. J. Physiol. Renal Physiol.* **302,** F1395–1401
43. Pisitkun, T., Bieniek, J., Tchapyjnikov, D., Wang, G., Wu, W. W., Shen, R. F., and Knepper, M. A. (2006) High-throughput identification of IMCD proteins using LC-MS/MS. *Physiol. Genomics* **25,** 263–276
44. Kortenoeven, M. L., Pedersen, N. B., Rosenbaek, L. L., and Fenton, R. A. (2015) Vasopressin regulation of sodium transport in the distal nephron and collecting duct. *Am. J. Physiol. Renal Physiol.* **309,** F280–F299
45. Staub, O., Dho, S., Henry, P., Correa, J., Ishikawa, T., McGlade, J., and Rotin, D. (1996) WW domains of Nedd4 bind to the proline-rich PY motifs in the epithelial Na^+ channel deleted in Liddle's syndrome. *EMBO J.* **15,** 2371–2380
46. He, Y. F., Bao, H. M., Xiao, X. F., Zuo, S., Du, R. Y., Tang, S. W., Yang, P. Y., and Chen, X. (2009) Biotin tagging coupled with amino acid-coded mass tagging for efficient and precise screening of interaction proteome in mammalian cells. *Proteomics* **9,** 5414–5424
47. Liang, S., Yu, Y., Yang, P., Gu, S., Xue, Y., and Chen, X. (2009) Analysis of the protein complex associated with 14-3-3ϵ by a deuterated-leucine labeling quantitative proteomics strategy. *J. Chromatogr. B Analyt. Technol. Biomed. Life Sci.* **877,** 627–634
48. Angrand, P. O., Segura, I., Völkel, P., Ghidelli, S., Terry, R., Brajenovic, M., Vintersten, K., Klein, R., Superti-Furga, G., Drewes, G., Kuster, B., Bouwmeester, T., and Acker-Palmer, A. (2006) Transgenic mouse proteomics identifies new 14-3-3-associated proteins involved in cytoskeletal rearrangements and cell signaling. *Mol. Cell Proteomics* **5,** 2211–2227
49. Lehoux, S., Abe, Ji., Florian, J. A., and Berk, B. C. (2001) 14-3-3 Binding to Na^+/H^+ exchanger isoform-1 is associated with serum-dependent activation of Na^+/H^+ exchange. *J. Biol. Chem.* **276,** 15794–15800